# 5

# Fructose : Conformational Properties of all Different Tautomers and Implications of their Lipophilicity Patterns on Sweetness

**Abstract:** A comprehensive force-field based conformational analysis of all different tautomeric forms of D-fructose was carried out. The β- and α-pyranoid forms exhibit opposite $^{2}C_{5}$- and $^{5}C_{2}$-ring geometries, respectively. Calculation of fully relaxed energy potential surfaces of the ring conformations of β- and α-D-fructofuranose, and their comparison with simple model compounds such as cyclopentanol and tetrahydro-2-furanol revealed $^{2}T_{3} \leftrightarrow E_{3} \leftrightarrow {}^{4}T_{3} \leftrightarrow {}^{4}E$ conformations to be energetically favorable in the case of the β-furanose, and preferred $E_{2} \leftrightarrow {}^{0}T_{2} \leftrightarrow {}^{0}E$ geometries for the α-furanose. The computational data is well in accord with statistical crystal structure analysis and solution conformations derived from $^{3}J_{H\text{-}H}$-NMR-coupling constants, indicating the relevance of the anomeric effect of the 2-OH group and the steric properties of the 1-$CH_2OH$ function for the observed conformational trends. NMR-parameters of acyclic *keto*-D-fructose derivatives point towards an almost linear extended zigzag carbon-chain as the minimum energy rotamer. Computation of molecular lipophilicity patterns (MLP's) mapped on the contact surfaces of all tautomers provides supportive evidence for the β-pyranose being the only sweet tasting compound, while all other isomers are substantially less sweet or devoid of any taste entirely. On the basis of the MLP's, a reassignment of the glucophoric system of β-D-fructopyranose was made: the 3,4-diol grouping interacting via hydrogen bondings with the sweetness receptor, while the surface area of 6-$CH_2$-$O_6$-1-$CH_2$ contributes to the hydrophobic part of the receptor affinity.

Against the background of the widespread utilization of the sweetest natural occurring sugar fructose for food purposes, either in pure crystalline form[168] or as high-fructose syrups[169], it is somehow surprising, how little information is still available on structure-sweetness relationships of this compound. In comparison to the large variety of commonly used sweeteners like sucrose, sucralose or synthetic high-potency sweeteners, which have only few degrees of conformational freedom, the situation becomes more complicate in the case of fructose: in solution a fast tautomerization yields a complex mixture of pyranoid and furanoid isomers[93-95] (Fig. 2-13 on p. 39), such that at least four components have to be included into detailed structure-sweetness considerations. However, so far all ideas rest on β-D-fructopyranose: freshly prepared solutions of the crystalline β-pyranoid form are almost twice as sweet as sucrose (1.8 x)[91,92], but when equilibration is complete, the solution is only slightly sweeter than one of sucrose of equal w/v-concentration[91].

This conclusion is supported by the temperature dependency of sweetness: shifting the tautomeric mixture with raising temperature towards higher proportions of entropy favored furanoid components[93-95] is accompanied by a decrease of sweetness[93,106]. Thus, the furanoid isomers appear to be substantially less sweet than the β-pyranoid form, or devoid of any taste altogether[93]. Actually, since the tautomerization is very fast and essentially complete within 10 min[93] even under neutral conditions and ambient temperature, nobody really knows the exact sweetness potency of pure β-D-fructopyranose. Non-neutral, physiological conditions have to be considered when focusing on the molecular mechanisms of sweet taste perception on the tongue, which might even dramatically increase tautomerization speed[175]. So probably all sweetness tests have been carried out with – at least partially – equilibrated solutions that contain considerable amounts of up to 25% of furanoid isomers.

In the preceding chapter a detailed review on structure-sweetness considerations of β-D-fructopyranose considering force-field calculations and molecular modelings of the electrostatic potential profiles and lipophilicity patterns on molecular surfaces was given. These rationalizations were additionally supported by calculation of energetically favorable molecular binding sites and relative sweetness potencies of a number of fructose derivatives. To obtain further corroborations for these concepts, a detailed molecular modeling study of all fructose tautomers and the resulting consequences on structure-sweetness relationships is presented in this chapter.

Prior to the discussion of the molecular modelings, the computational evaluation of the conformational properties for all tautomers should be discussed, focusing especially on the geometries of the furanoid five-membered rings, and their comparison with NMR-data and statistical crystal structure analysis.

## Pyranoid Fructose Tautomers – β- and α-D-Fructopyranose

Crystalline fructose has been studied by X-ray[89] and neutron diffraction[90] structure analysis, showing the β-pyranoid form to represent the solid state isomer. Here, β-D-fructopyranose adopts the $^2C_5$-ring conformation, which is also being retained in solution. In the crystalline state, the hydroxymethyl group exhibits a *gauche-gauche* arrangement[102] relative to the pyranoid ring. Extensive AM1-based semiempirical[99,100] and *ab initio*[98,103] calculations had been carried out on this fructose tautomer, as well as a detailed PIMM88-force field[45] based analysis (cf. Chapter 4). Here, of the three possible $CH_2OH$-conformations, the *tg* conformer emerges as the global energy minimum form due to its stabilization by an 1-OH ··· O-3 intramolecular hydrogen bond which overcomes the unfavorable 1,3-diaxial like interactions between O-1 and O-3. In solution, the hydroxyl groups can satisfy their

hydrogen bond requirements by solvation, such that only the *gg* and the *gt* conformations of the 1-$CH_2OH$ group[102] are populated[70-73]. In Fig. 5-1**A**, the force field optimized solid state geometry of β-D-fructopyranose is shown as a ball and stick model.

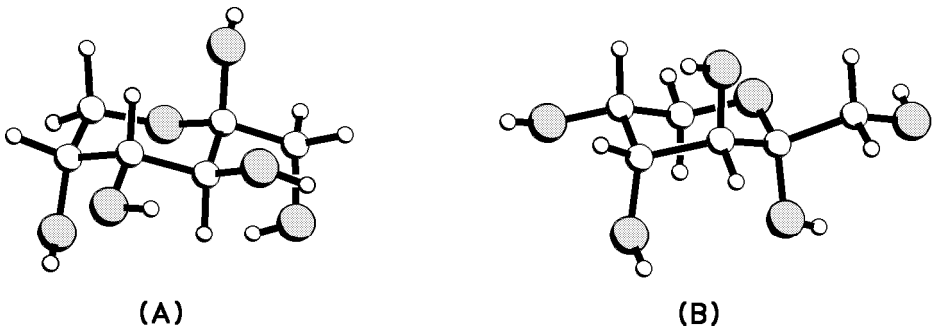


**Fig. 5-1.** Force field optimized solid state $^2C_5$-conformation of β-D-fructopyranose (**A**), and low energy conformation of α-D-fructopyranose (**B**), exhibiting an inverted $^5C_2$-ring geometry.

In contrast to the β-D-form, the force field based conformational analysis of α-D-fructopyranose showed the inverted $^5C_2$-ring conformation to be more stable than the $^2C_5$-form. The opposite conformational preferences of the β- and α-pyranoid forms can be traced back to the anomeric effect[193] of the axial-oriented 2-OH group, as well as the equatorial arrangement of the larger hydroxymethyl unit in both cases. These results are further supported by $^1$H-NMR spectroscopical data of tetra-*O*-acyl fructopyranosides Table 5-1)[194-197]: the rather large $J_{3,4}$-coupling constants for the β-pyranosides ($J \approx 10 - 11$ Hz) disclose antiperiplanarity of H-3 and H-4, whilst the small values of $J_{5,6A}$ and $J_{5,6B}$ ($\approx 1 - 2$ Hz) reveal an equatorial-equatorial (e,e) and equatorial-axial (e,a) relationship of the respective protons. Similarly, the small $J_{4,5}$-couplings are in accord with an a,e-arrangement of H-4 and H-5. However, the $^1$H-NMR-coupling patterns in the α-series can only be reconciled with a $^5C_2$-ring conformation, as evidenced by both the small values of $J_{3,4}$ and $J_{4,5}$ ($\approx 3 - 4$ Hz, *gauche*-type e,e- and e,a-relationships, respectively). In addition, the large coupling $J_{5,6A} \approx 10 - 11$ Hz is only consistent with an a,a-arrangement of H-5 and H-$6_A$.

As already outlined above, assessment of the conformational preferences of the $CH_2OH$-group in α-D-fructopyranose by permutation of all free torsion angles (i.e. computation of all possible combinations of staggered conformations) using *in vacuo*-force field calculations is misleading: again the global minimum energy geometry is being characterized by an intramolecular hydrogen bond between O-1 and O-3 (*gg* arrangement of the $CH_2OH$-unit). This H-bond will certainly be disintegrated by

solvation in aqueous solutions in order to avoid the unfavorable 1,3-diaxial like interactions between both oxygen atoms. In Fig. 5-1 **B**, the lowest energy conformation with no intramolecular hydrogen bonds is shown as a molecular model for α-D-fructopyranose.

**Table 5-1.** $^1$H-$^1$H-ring coupling constants (300 MHz, $CDCl_3$) of β- and α-d-fructopyranose derivatives.

| compound | | X | R | $^1$H-$^1$H-coupling constants [Hz] $J_{3,4}$ | $J_{4,5}$ | $J_{5,6A}$ | $J_{5,6B}$ | ring | ref. |
|---|---|---|---|---|---|---|---|---|---|
| **β-D-fructopyranosyl derivatives:** | | | | | | | | | |
| 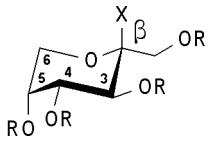 | **1** | Cl | Ac | 10.0 | 3.4 | 1.4 | 1.7 | $^2C_5$ | 194 |
| | **2** | OH | Ac[a)] | 10.5 | 3.5 | 1.1 | 2.1 | $^2C_5$ | 195 |
| | **3** | OMe | Ac | 10.0 | 3.6 | 1.2 | 1.6 | $^2C_5$ | 195 |
| | **4** | OAc | Ac | 10.7 | 3.5 | 1.5 | 2.0 | $^2C_5$ | 195 |
| | **5** | H | Bz | 10.0 | 3.4 | -[b)] | -[b)] | $^2C_5$ | 194 |
| | **6** | Cl | Bz | 10.2 | 3.3 | 1.1 | 1.9 | $^2C_5$ | 194 |
| | **7** | Br | Bz | 10.0 | 3.3 | 1.0 | 1.7 | $^2C_5$ | 194 |
| | **8** | I | Bz | 10.0 | -[b)] | 1.0 | 1.6 | $^2C_5$ | 194 |
| | **9** | OH | Bz | 10.5 | 3.4 | 1.1 | 1.8 | $^2C_5$ | 194 |
| | **10** | OMe | Bz | 10.0 | 3.0 | -[b)] | -[b)] | $^2C_5$ | 196 |
| | **11** | OBz | Bz | 10.5 | 3.3 | 1.3 | 1.7 | $^2C_5$ | 194 |
| | **12** | OAc | Bz | 9.9 | 3.2 | 0.8 | 1.3 | $^2C_5$ | 194 |
| | **13** | CN | Bz | 10.2 | 3.3 | 1.3 | 1.3 | $^2C_5$ | 197 |
| **α-D-fructopyranosyl derivatives:** | | | | | | | | | |
| 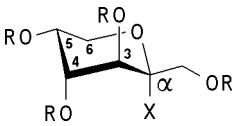 | **14** | OAc | Ac | 3.8 | 3.6 | 10.4 | 5.2 | $^5C_2$ | 194 |
| | **15** | I | Bz | 3.2 | 3.4 | 10.6 | 5.3 | $^5C_2$ | 194 |
| | **16** | OBz | Bz | 3.7 | 3.5 | 10.5 | 5.2 | $^5C_2$ | 194 |
| | **17** | OAc | Bz | 4.2 | 3.4 | 9.9 | 5.0 | $^5C_2$ | 194 |
| | **18** | CN | Bz | 3.7 | 3.3 | 11.3 | 5.2 | $^5C_2$ | 197 |

a) $C_6D_6$. – b) not determined.

## Furanoid Fructose Tautomers – β- and α-D-Fructofuranose

### *Conformations of Five-Membered Ring Systems*

The conformational properties of five-membered rings can be described by the concept of pseudorotation[198]: ten twist (T, $C_2$-symmetry) and envelope (E, $C_s$-symmetry) conformations each, which can be characterized by the Altona-Sundaralingam[199] or the Cremer-Pople[122] puckering parameters, both formalisms being almost equivalent[200]. The latter are used in this study: the puckering angle ϕ indicates the type of conformation (cf. Fig. 5-2) and the puckering amplitude $q$ serves as a measure of ring distortion. Interconversion of the different

conformations involves small successive displacements of the ring atoms below or above the mean ring plane, or in other terms, continuous minor changes of the ring torsion angles that indicate the high flexibility of these rings.

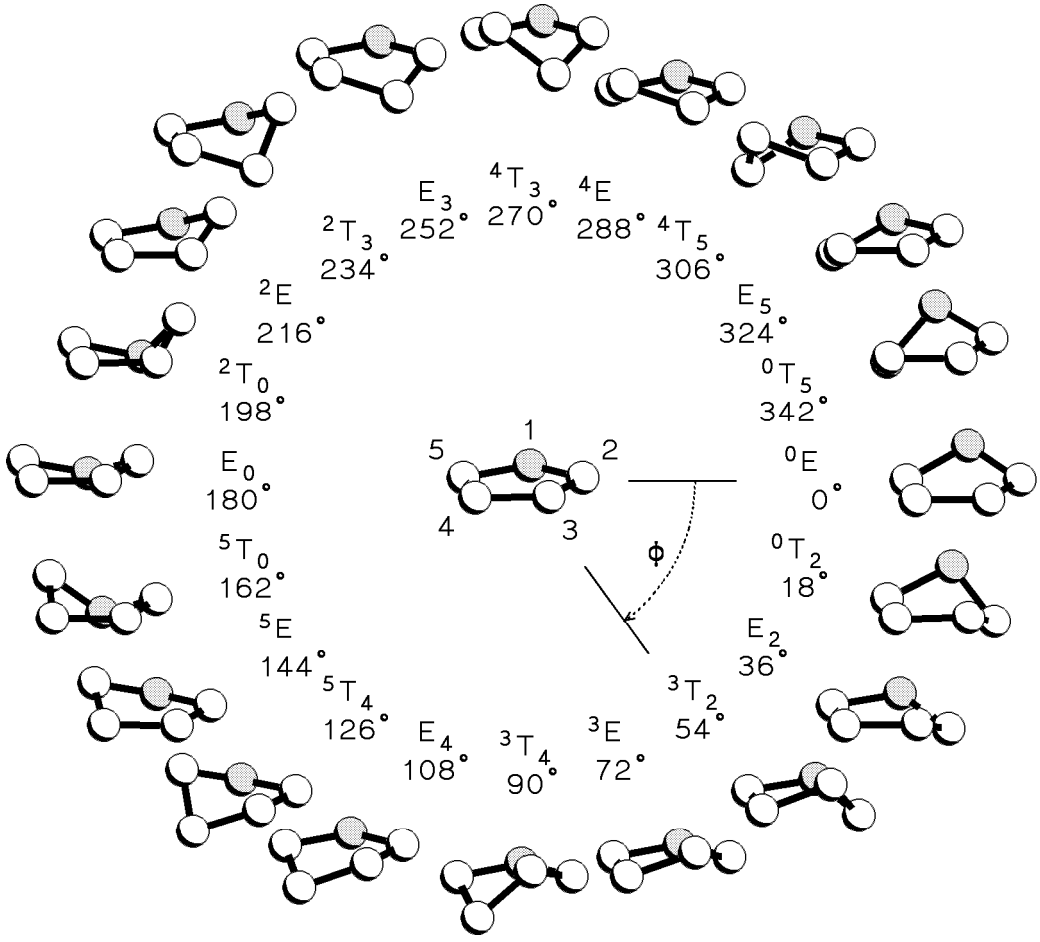


**Fig. 5-2.** Itinerary of pseudorotation of furanose ring systems, the Cremer-Pople puckering parameter $\phi$ is indicated for the different twist (T) and envelope (E) conformations (puckering amplitude $q \approx 0.45$), molecules are plotted in respect to a constant viewpoint.

The conformational analysis and the calculation of energy potential surfaces of furanoid ring systems can be carried out either in terms of two ring-torsion angles or of the Cremer-Pople puckering angle and amplitude. Both parameter-sets also depend on bond-angles and -lengths, the error introduced by those simplifications certainly being less than the one in energy calculation. However, in contrast to earlier calculations[201,202] torsion angles were used as ring descriptors, since they are more conveniently handled with the force field program and finally yield an orthogonal rather than a polar coordinate data set for the contour plots. The

$\Phi$ ($O_5$-$C_2$-$C_3$-$C_4$) / $\Psi$ ($C_3$-$C_2$-$O_5$-$C_5$) pair of torsion angles was chosen, since it is the most sensitive one towards conformational changes at the C-2-anomeric center.

*Conformational Properties of Cyclopentanol and Tetrahydro-2-furanol in Relation to the Anomeric Effect*

The anomeric effect[193] must be regarded as a strong conformation influencing force in carbohydrate structures, being even more pronounced in furanoid than in pyranoid structures[203,204]. The PIMM88-force field[45] used here was shown to properly reproduce the conformational preferences and the anomeric and exoanomeric effects in acyclic and cyclic acetal structures such as dimethoxy methane, dihydroxy methane, and tetrahydro-pyranosides[162]. To get an anticipation of the conformational trends induced by this effect in the furanose series, the model substances cyclopentanol as well as its half-acetalic analog tetrahydro-2-furanol were analyzed in terms of their $\Phi$ / $\Psi$-energy potential surfaces (Fig. 5-3 and 5-4).*

Both contour maps are scaled relative to their global energy minimum, resembling closely each other. They both exhibit two oppositely located local energy minima, which correspond to different conformers with a pseudoaxial ($^2T_3$ ring conformation, upper left) or pseudoequatorial ($^3T_2$ form, lower right) arrangement of the hydroxyl ring substituent. In both cases, the ring shaped contour of 5 – 10 kJ/mol delineates the pathway of pseudorotation in terms of the $\Phi$ / $\Psi$-torsion angles, indicating the very low energy barrier for the interconversion of both conformers. The center energy maximum represents the planar structure +27.9 and +22.8 kJ/mol above the global energy minimum, respectively. However, the conformational preferences of both compounds are strikingly different. In the case of the cyclopentane-2-ol the pseudoequatorial arrangement of the OH-group emerges to be 3.6 kJ/mol more stable than the pseudoaxial conformer. The opposite situation is calculated for the oxy-analog tetrahydro-2-furanol: the anomeric effect overcomes the unfavorable steric interactions of a pseudoaxial oriented hydroxyl group, thus the $E_2$-conformation (slightly distorted towards $^3T_2$) being 1.2 kJ/mol less stable than the inverse $^2T_3$-geometry. The integral populations calculated from the percentage distribution plots (Fig. 5-3 and 5-4) indicate a 20 : 80 preference of the conformer with a pseudoequatorial OH-group over

* To maintain consistency throughout all conformational labels used within this report, all furanoid rings were numbered according to the fructose nomenclature (O-$C_2$-$C_3$-$C_4$-$C_5$), which also applies to non-carbohydrate compounds like tetrahydro-2-furanol. To further unify the ring numbering with C-2 representing the anomeric center in all cases, the carbocyclic analog was numbered as cyclopentane-2-ol ($C_1$-$C_2$(OH)-$C_3$-$C_4$-$C_5$), which is not in accord with IUPAC rules. The conformational designation is that recommended by the IUPAC-IUB Joint Commission on Nomenclature, *Europ. J. Biochem.* **1980**, *111*, 295-298; *Pure Appl. Chem.* **1981**, *53*, 1901-1905. The top and bottom ring sides are defined by clockwise and anticlockwise numbering schemes.

a pseudoaxial arrangement for cyclopentanol, being inverted to a 60 : 40 ratio for tetrahydro-2-furanol. Those ratios are consistent with the calculated single-conformer energy differences of -3.6 and 1.2 kJ/mol, respectively. The molecular parameters and conformations of the calculated local energy minimum structures are summarized in Table 5-2. The variation of ring conformation introduced by small changes of torsion angles ±40° indicates the high flexibility of five-membered rings. Additional support for the validity of the energy potential surfaces is found by *in vacuo* molecular dynamics simulations at 300 K showing almost free pseudorotation to occur in the ps-range.

Essentially free pseudorotation was observed for cyclopentane by thermodynamic[198,205], RAMAN[206], IR[207-211], electron diffraction[212], and computational studies[213-220], with an almost vanishing small barrier (≤ 0.02 – 0.05 kJ/mol[215,219]), and a central plateau of ≈ 1800 $cm^{-1}$ (22.6 kJ/mol[211], exp. and calc. values range from 19.6 – 23.1 kJ/mol[205,206,215,218]), the average atomic displacement from planarity was determined to be approx. 0.43 – 0.48 Å[205-207,212]. For tetrahydrofuran[209,214,215,218,221-224], the ring inversion via the planar conformation was found to be approx. 1220 $cm^{-1}$ (14.6 kJ/mol)[215,218,222] more unfavorable than pseudorotation, which occurs with a very low barrier of ≈ 57 $cm^{-1}$ (0.7 kJ/mol)[221,222] only. The tetrahydrofuran ring is less puckered than cyclopentane[224], the ring torsion angles were estimated to be within the range of -40 – +40°[223]. From the temperature dependency of vicinal coupling constants in THF it must be concluded that at least two different conformations of unequal energy coexist in an equilibrium mixture[224]. Substitution of cyclopentane presumably yields higher barriers of pseudorotation[205]: band-broadening and splitting of IR low frequency vibrations in cyclopentanol[225,226] was interpreted in terms of the presence of two different conformers with a pseudoequatorial-OH preferred over a pseudoaxial substituent[225], and a pseudorotational barrier of less than 8 kJ/mol[226]. For tetrahydro-2-furanol – which is preferred over its acyclic tautomer 4-hydroxy-butyraldehyde in solution[227,228] – no such studies have been put forth.

In summary, the calculated data for cyclopentanol and tetrahydro-2-furanol is well in accord with all of these experimental facts. The lower puckering amplitude as well as the lower barrier to planarity of the tetrahydrofuran ring as compared to its carbo-cyclic analog is correctly predicted, the calculated pseudorotational barrier of $\Delta H^{\neq} \approx 5 - 10$ kJ/mol – the effective free energy barrier $\Delta G^{\neq}$ might even be lower – fits the IR-based results. At least in the case of cyclopentanol, the proposed presence of two different conformers has been confirmed experimentally. The observed opposite conformational trends predict the strong anomeric effect in furanoid rings[203,204] as a pronounced conformation influencing force.

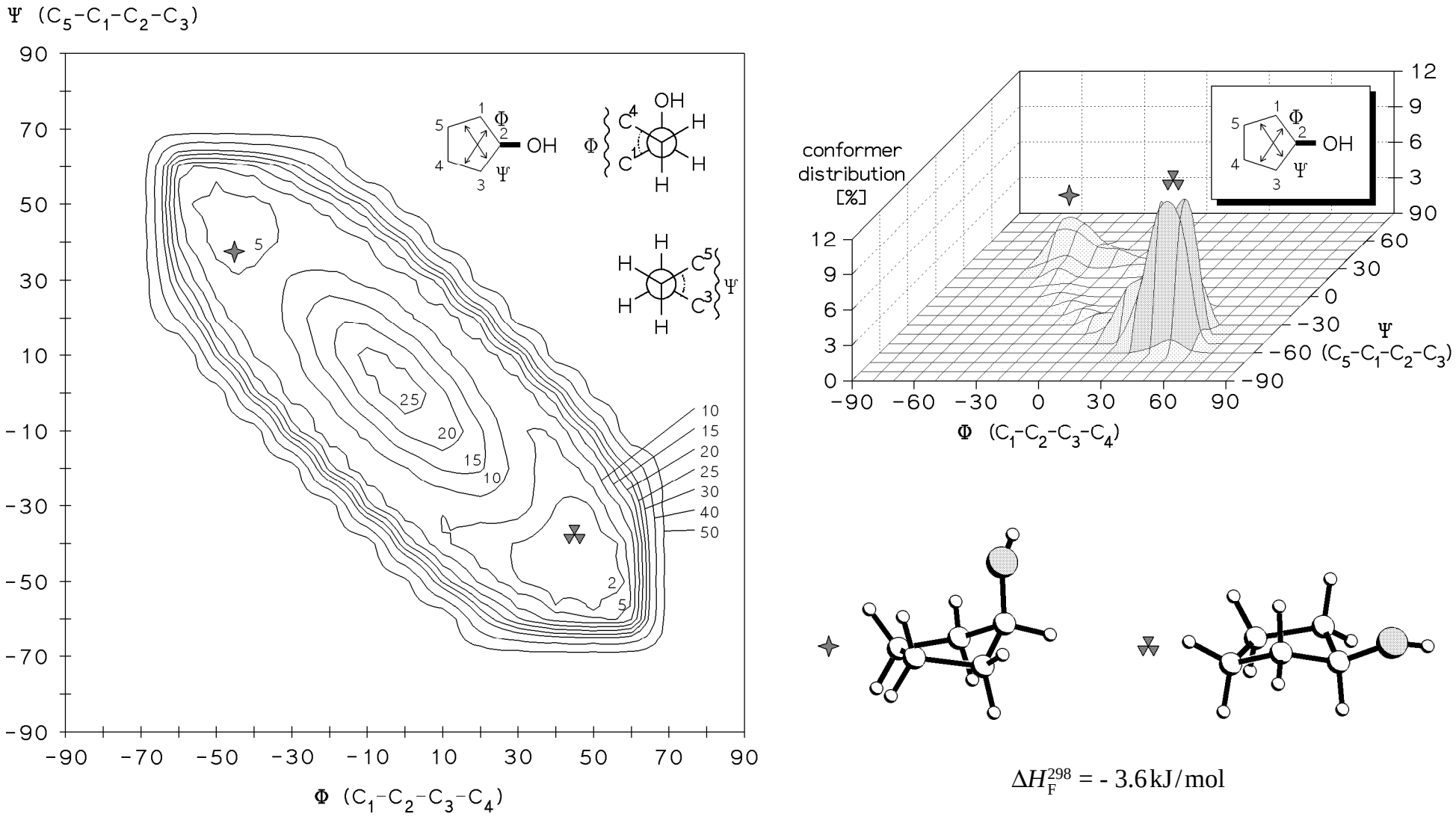


**Fig. 5-3.** PIMM88-force field[45] derived energy potential surface of cyclopentane-2-ol as a function of the ring torsion angles Φ and Ψ, energies are given in kJ/mol relative to the global minimum. The asterisks mark the conformations of the minimum energy structures shown on the *right* side, the pseudoequatorial conformer being 3.6 kJ/mol more stable than the pseudoaxial one (symmetrical conformations of same energy are not marked). In addition, a three-dimensional plot of the percentage distribution according to the Boltzmann equation at 25°C is given.

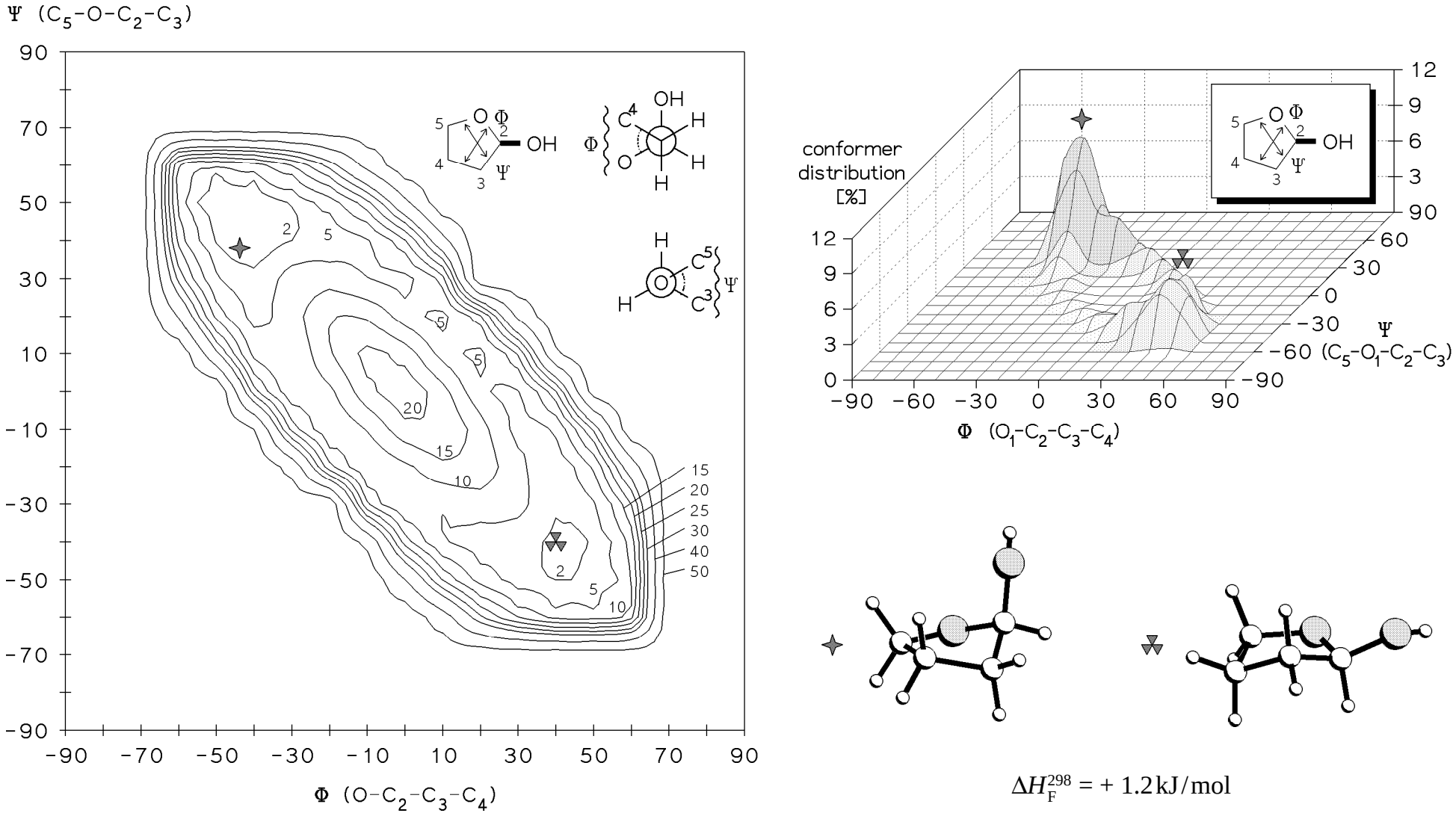


**Fig. 5-4.** Energy potential surface (kJ/mol relative to the global minimum) and 3D-plot of percentage conformer distribution (at 25°C) of (*R*)-tetrahydro-2-furanol as a function of the ring torsion angles Φ and Ψ. Due to the anomeric effect, the pseudoaxial conformer emerges from the calculation to be 1.2 kJ/mol more stable than the pseudoequatorial one.

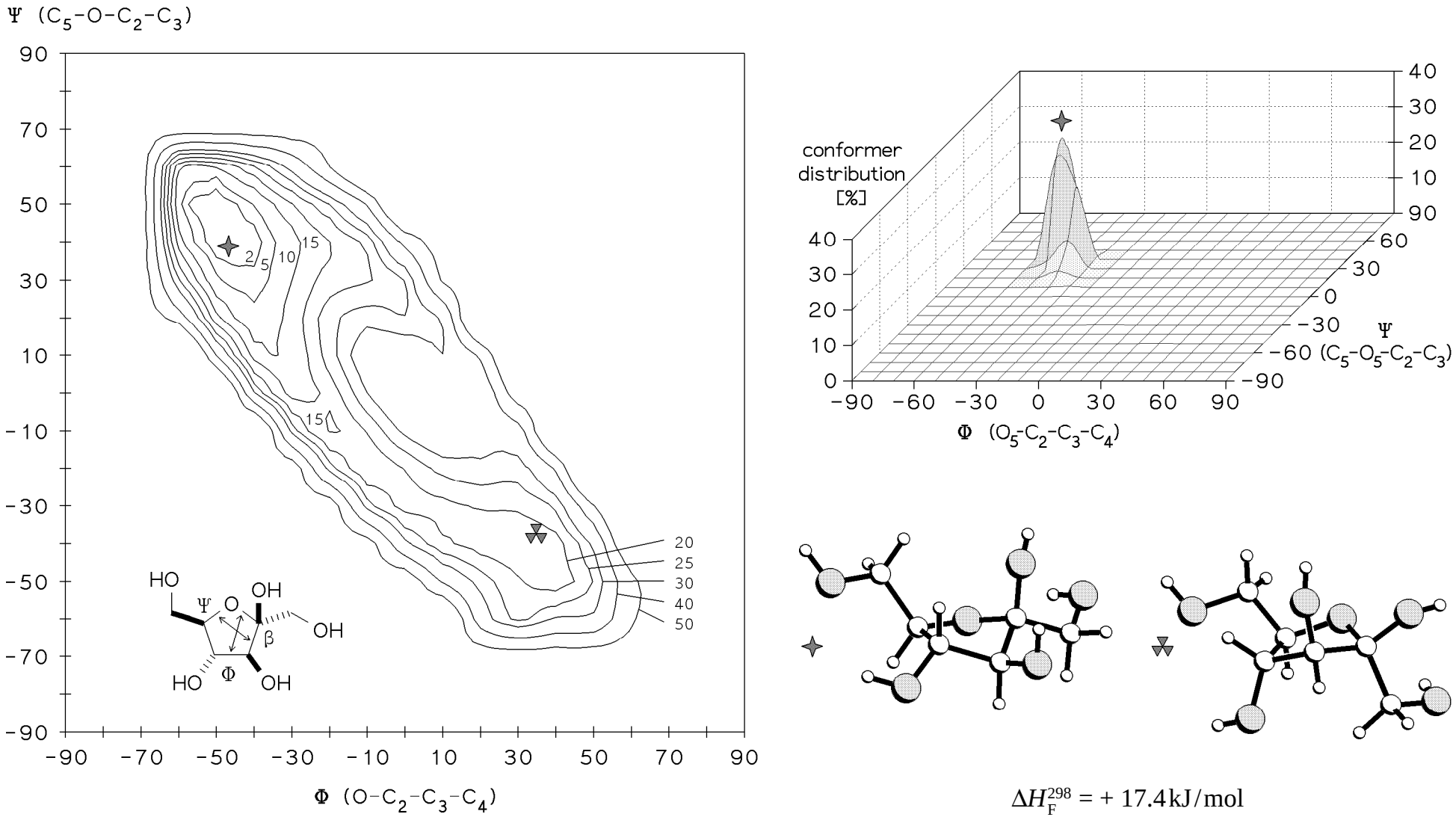


**Fig. 5-5.** Energy potential surface (kJ/mol relative to the global minimum) and 3D-plot of percentage conformer distribution (at 25°C) of β-D-fructofuranose as related to the ring torsion angles Φ and Ψ.

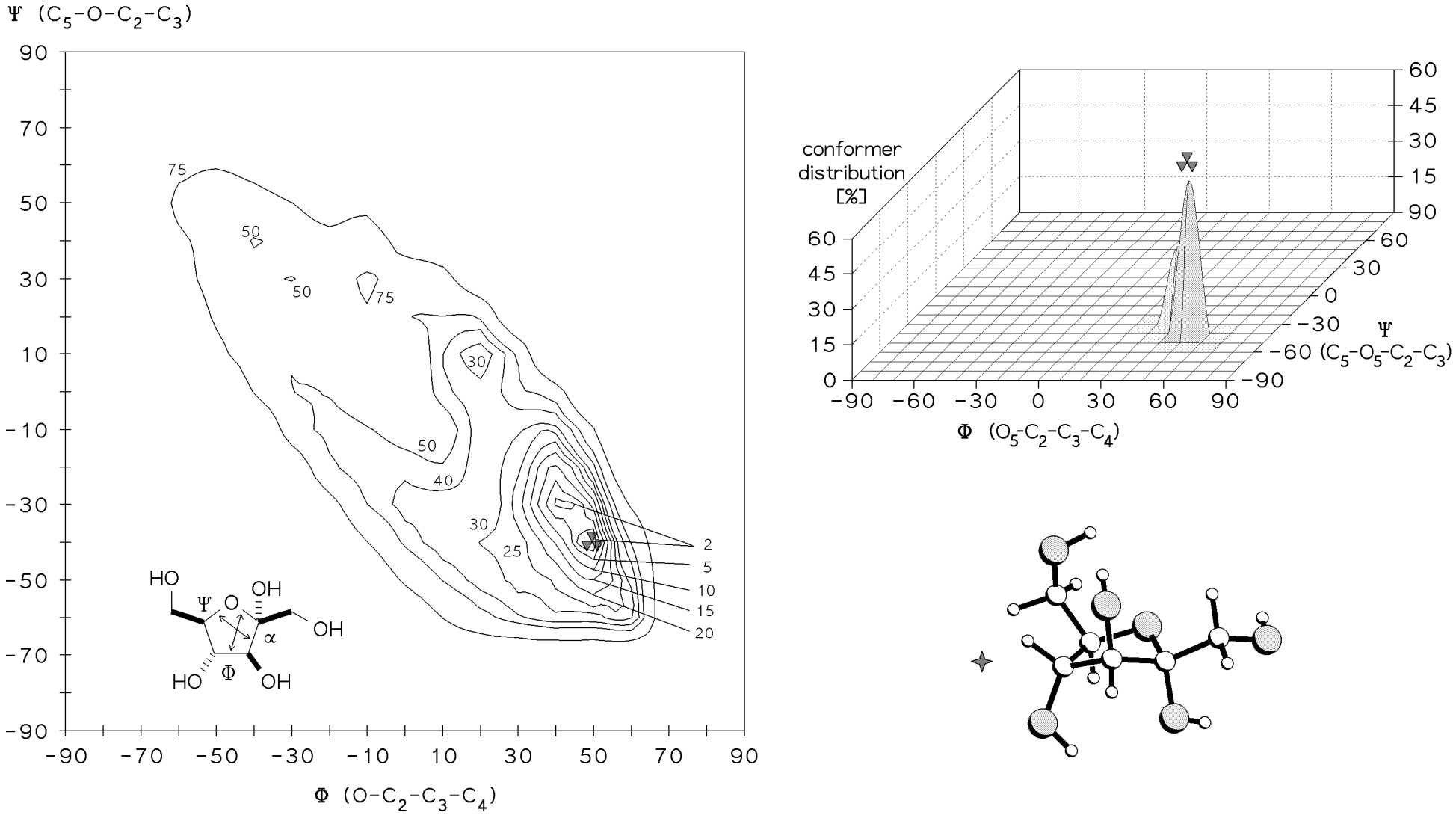


**Fig. 5-6.** Φ / Ψ-Energy potential surface (kJ/mol relative to the global minimum) and 3D-plot of percentage conformer distribution (at 25°C) of α-D-fructofuranose.

**Table 5-2.** Calculated and experimental geometry parameters and conformations of five-membered ring compounds.

| compound | | $\Delta H_F^{298}$ [kJ/mol] | Cremer-Pople-Par.[a] $\phi$ | $q$ | torsion angles[b] $\Phi$ | $\Psi$ | conformation[c] |
|---|---|---|---|---|---|---|---|
| cyclopentane[212,214,217,219] | exp. | 0.02[219] | 54.0 | 0.415[i] | 42.5 | -34.5[d] | $^3T_2$[f] |
| | | | 36.0 | 0.415[i] | 40.5 | -40.5[e] | $E_2$[f] |
| cyclopentane-2-ol[g] |  | -3.6 | 232.1 | 0.442 | -45.2 | 37.5 | $^2T_3$ ($\equiv$ $^2T_1$)[h] |
| | | | 51.6 | 0.439 | 44.9 | -37.5 | $^3T_2$ ($\equiv$ $^1T_2$)[h] |
| tetrahydrofuran[214] | exp. | ≈0.7[222] | 0.0 | 0.364[i] | 23.0 | -39.2 | $^0E$ ($\equiv$ $E_0$)[h] |
| | | | 90.0 | 0.355[i] | 29.6 | -11.5 | $^3T_4$ ($\equiv$ $^4T_3$)[h] |
| (*R*)-tetrahydro-2-furanol |  | 1.2 | 236.5 | 0.422 | -43.8 | 36.6 | $^2T_3$ |
| | | | 43.3 | 0.392 | 40.1 | -39.9 | $E_2$ ($\rightarrow$ $^3T_2$) |
| β-D-fructofuranose |  | 17.4 | 237.2 | 0.457 | -46.9 | 39.0 | $^2T_3$ ($\rightarrow$ $E_3$) |
| | | | 37.2 | 0.350 | 34.7 | -37.3 | $E_2$ |
| α-D-fructofuranose |  | - | 56.5 | 0.476 | 49.7 | -40.2 | $^3T_2$ |

a) puckering angle $\phi$ and amplitude $q$ according to Fig. 5-2[122,123]. – b) ring torsion angles F ($X\text{-}C_2\text{-}C_3\text{-}C_4$) and Y ($C_3\text{-}C_2\text{-}X\text{-}C_5$) with $X = C_1$ (cyclopentane rings) or $X = O$ (tetrahydrofuran rings). – c) the main conformation and the direction of distortion are given. – d) $F = +w_3$, $Y = -w_2$[217,219]. – e) $F = +w_1$, $Y = -w_1$[217,219]. – f) and symmetry related conformations. – g) ring numbering not according to IUPAC. – h) symmetry properties. – i) recalculated from reported bond and torsion angles using standard bond lengths ($r_{C\text{-}C} \approx 1.54$ Å, $r_{C\text{-}O} \approx 1.43$ Å)[223].

*Energy Potential Surfaces of* β- *and* α-D-*Fructofuranose*

The overall shapes of the fully relaxed energy potential surfaces of β- and α-D-fructofuranose (Fig. 5-5 and 5-6) resemble only roughly to those of the simple model compounds presented above. For β-D-fructofuranose two local energy minima are observed, a large extended one (Fig. 5-5, upper left) which corresponds to a slightly distorted $^2T_3$-ring conformation, and a very shallow one +17.4 kJ/mol above the global minimum ($E_2$-conformation, lower right). From the three-dimensional plot of the percentage conformer distribution (Fig. 5-5) it becomes obvious that only one relevant geometry has to be considered. The chiral properties of this compound lead to a striking asymmetry of the energy potential surface and a considerably restricted pathway of pseudorotation. Most notably, the relevant upper left energy minimum is extended in an asymmetric fashion towards $^4T_3$-ring conformations.

For α-D-fructofuranose a single energy minimum is computed (Fig. 5-6), which is located in the opposite conformational region. The axial arrangement of the anomeric hydroxyl group as well as the pseudoequatorial orientation of the larger $CH_2OH$-group lead to the preference of the $^3T_2$-conformation for this compound.

The conformational properties of β-D-fructofuranose (Fig. 5-5) and (*R*)-tetrahydro-2-furanol (Fig. 5-4) correspond to each other, such that the global energy minima are located within similar regions of the energy potential surfaces. The opposite trend observed for α-D-fructofuranose (Fig. 5-6) must be related to the mirror image of the model compound, i.e. (*S*)-tetrahydro-2-furanol: the symmetry properties of both compounds require mirroring the contour plot of Fig. 5-4 (and the conformational labels!) in respect to the origin of the Φ / Ψ-coordinate system, thus the energy minima coinciding in this case, too.

It should be noted that the ring torsion angles predicted by the PIMM88-force field are probably slightly overestimated by approx. 5° as compared with the experimental values observed for cyclopentane (cf. Table 5-2).

*Statistical Crystal Structure Analysis*

Further corroboration up to the relevance of the calculated conformation can be obtained from solid-state structure analysis of fructofuranosyl compounds from the Cambridge Crystallographic database[192]. In Table 5-3 and Fig. 5-7, a comprehensive list of the chemical formulas and molecular parameters (Table 5-4)[25,229-263] of crystallographically characterized compounds is given, including some constrained structures with fused ring units as well as three α-L-sorbofuranosyl compounds.

In Fig. 5-8, a general two-dimensional correlation of the Φ / Ψ-torsion angles and the Cremer-Pople parameters ϕ and *q*, as calculated for furanose rings is presented as a contour plot, in conjunction with a scatter plot of the furanose conformations derived from these solid state structures. For constant puckering amplitudes *q*, the ring torsion angles were shown to depend in a cosinusoidal fashion from the puckering phase angle ϕ[199,264]. The extended universal relationship ϕ, *q* = f(Φ / Ψ) can be directly superimposed on the energy potential surfaces for furanoid ring systems presented in Fig. 5-4 – 5-6, thus allowing a direct assignment of the molecular conformations to distinctive regions of the Φ / Ψ-plots. Due to the weak dependency of the Cremer-Pople parameters on bond-lengths and -angles it also applies – at least roughly – to the energy map of the cyclopentane ring system (Fig. 5-3).*

The solid state conformations of a large number of β-D-fructofuranoses indicate an unequivocal preference of $^{2}T_{3} \leftrightarrow E_{3} \leftrightarrow {}^{4}T_{3} \leftrightarrow {}^{4}E$ ring geometries ($\phi \approx 230 - 290°$)

* The deviation of the ϕ-contours for the $E_2$- (ϕ = 36°) and $^2E$-ring conformations (ϕ = 216°) from the mean diagonal line Φ = –Ψ in Fig. 5-8 must be attributed to the effect of different bond-lengths in furanose rings, thus indicating that the Cremer-Pople parameters[122,123] are not an exact – but nevertheless most versatile – descriptor of ring conformations.

with puckering amplitudes in the range of $q \approx 0.28 - 0.45$, thus fitting the calculated global minimum of the energy potential surface of the parent compound (Fig. 5-5).

**Table 5-3.** Substitution patterns of fructofuranose derivatives studied by crystal structure analysis.

| compound | | | $R^1$ | $R^2$ | $R^3$ | $R^4$ | $R^5$ |
|---|---|---|---|---|---|---|---|
| **β-D-fructofuranosyl derivatives:** | | | | | | | |
| -6-phosphate | **19** | | H | H | H | H | $PO_3Na_2$ |
| -6-phosphate | **20** | | H | H | H | H | $PO_3K_2$ |
| -1,6-diphosphate | **21** | | $PO_3HNa$ | H | H | H | $PO_3Na_2$ |
| | **22** | | - $C(CH_3)_2$ - | | H | H | Bz |
| Sucrose | **26** | | H | αGlc*p* | H | H | H |
| Xylo-sucrose | **32** | | H | αXyl*p* | H | H | H |
| Isomaltulose | **35** | | H | H | H | H | αGlc*p* |
| Lactulose | **36** | | H | βGal*p*- | H | H | H |
| | | | | (1→4)-Glc*p* | | | |
| Erlose | **37** | | H | αGlc*p*- | H | H | H |
| | | | | (1→4)-Glc*p* | | | |
| Melezitose | **38** | | H | αGlc*p* | αGlc*p* | H | H |
| Planteose | **39** | | H | αGlc*p* | H | H | βGal*p* |
| 1-Kestose[a)] | **40** | A | βFru*f* | αGlc*p* | H | H | H |
| | | B | H | αGlc*p*- | H | H | H |
| | | | | (1→2)-βFru*f*-1- | | | |
| 6-Kestose[a)] | **41** | A | H | αGlc*p* | H | H | βFru*f* |
| | | B | H | αGlc*p* | H | H | H |
| | | | | (1→2)-βFru*f*-6- | | | |
| Nystose[a)] | **42** | A | βFru*f* | αGlc*p* | H | H | H |
| | | | (1→2)-βFru*f* | | | | |
| | | B | βFru*f* | αGlc*p*- | H | H | H |
| | | | | (1→2)-βFru*f*-1- | | | |
| | | C | H | αGlc*p*- | H | H | H |
| | | | | (1→2)-βFru*f*-(1→2)-βFru*f*-1- | | | |
| Raffinose | **43** | | H | αGal*p*- | H | H | H |
| | | | | (1→6)-αGlc*p* | | | |
| Stachyose | **44** | | H | αGal*p*- | H | H | H |
| | | | | (1→6)-αGal*p*-(1→6)-αGlc*p* | | | |
| Cycloinulohexaose | **45** | | - [(1→2)-βFru*f*]$_5$ - | | H | H | H |
| **α-D-fructofuranosyl derivatives:** | | | | | | | |
| -pentabenzoate | **48** | | Bz | Bz | Bz | Bz | Bz |

a) Different fructofuranose ring systems per molecule.

**general formula:**

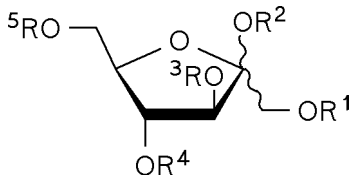

**Fructofuranosyl compounds:**

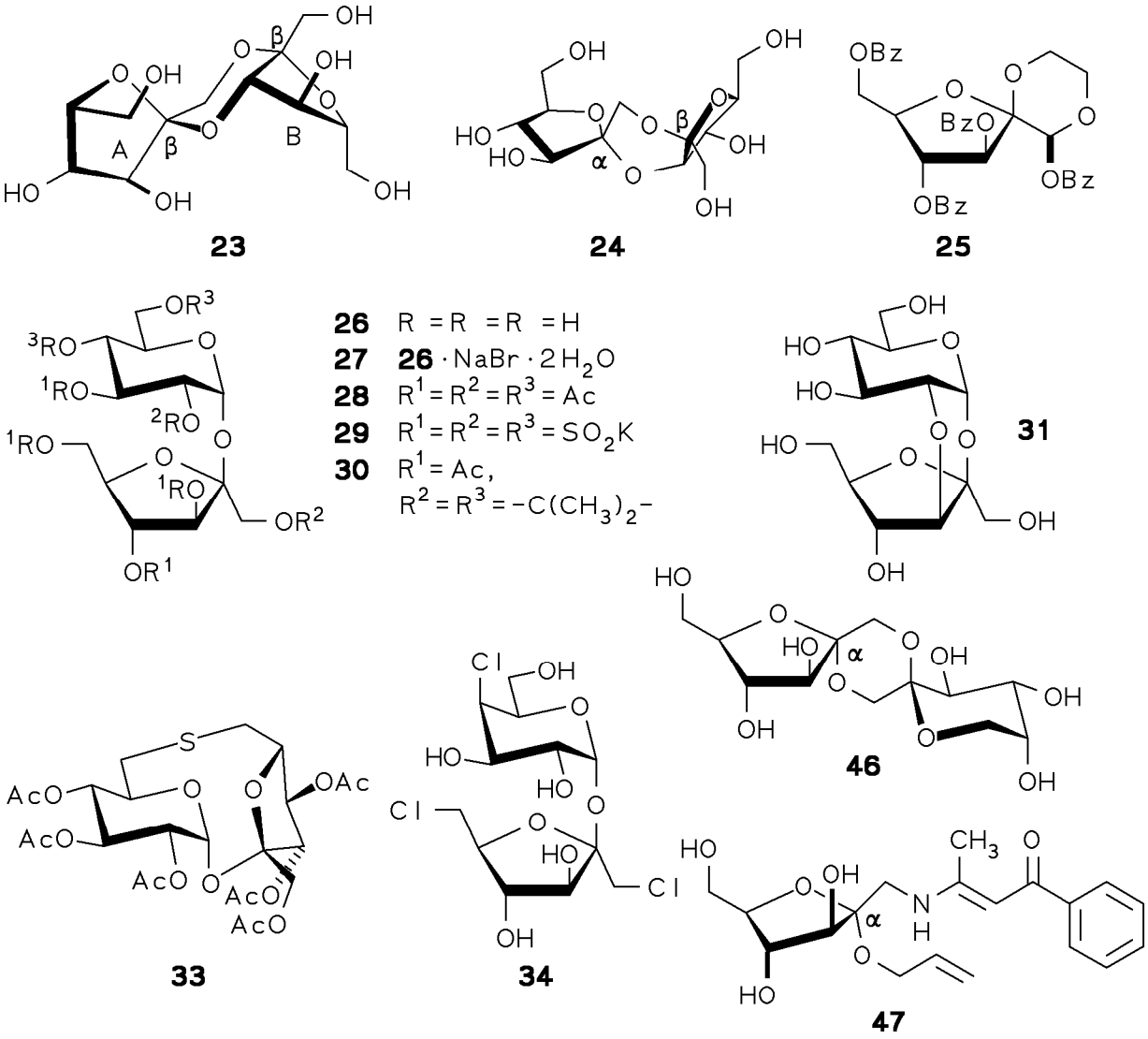


**Sorbofuranosyl compounds:**

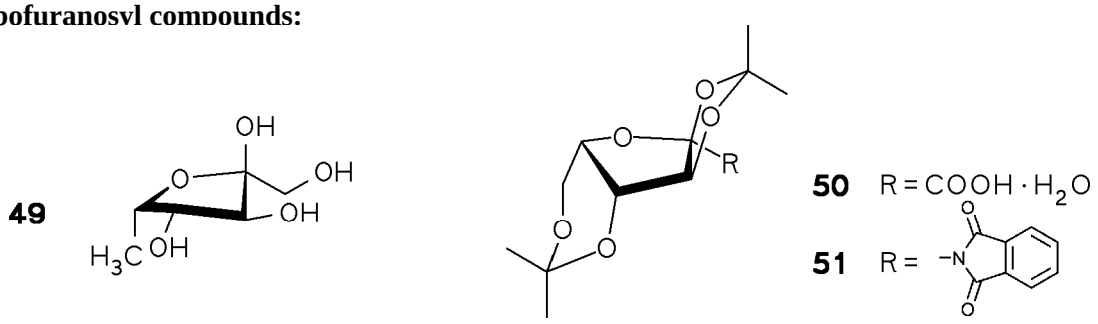


**Fig. 5-7.** Formulas of some crystallographically characterized fructo- and sorbofuranosyl compounds.

**Table 5-4.** Crystal conformations of β-D-fructofuranosyl- (**19** – **45**), α-D-fructofuranosyl- (**24α**, **46** – **48**), and α-L-sorbofuranosyl-compounds (**49** – **51**).

| compound | | Cremer-Pople-Par.[a] ϕ | *q* | torsion angles[b] Φ | Ψ | conformation[c] | CCDF-set[d] | ref. |
|---|---|---|---|---|---|---|---|---|
| **β-D-fructofuranosyl derivatives:** | | | | | | | | |
| **19** | | 236.0 | 0.330 | -34.3 | 28.5 | $^2T_3$ ($\rightarrow E_3$) | FAVBOT | 229 |
| **20** | | 244.1 | 0.359 | -37.2 | 27.6 | $E_3$ ($\rightarrow {}^2T_3$) | DEFLAB | 230 |
| **21** | | 254.8 | 0.374 | -36.3 | 22.1 | $E_3$ ($\rightarrow {}^4T_3$) | COWDOH01 | 231 |
| **22** | | 256.3 | 0.417 | -40.4 | 23.5 | $E_3$ ($\rightarrow {}^4T_3$) | GAFVUE | 232 |
| **23** | A | 215.5 | 0.365 | -37.1 | 39.0 | $^2E$ | SANXEK[e] | 233 |
| | B | 59.1 | 0.346 | 36.7 | -28.8 | $^3T_2$ ($\rightarrow {}^3E$) | | |
| **24** | β | 317.3 | 0.250 | -2.5 | -14.6 | $E_5$ ($\rightarrow {}^4T_5$) | BIVZAH | 234 |
| **25** | | 208.9 | 0.346 | -33.6 | 38.5 | $^2E$ ($\rightarrow {}^2T_0$) | –[g] | 235 |
| **26** | | 265.3 | 0.354 | -33.2 | 14.7 | $^4T_3$ ($\rightarrow E_3$) | SUCROS04 | 25 |
| **27** | I | 289.0 | 0.341 | -21.1 | -1.5 | $^4E$ | SUCNAB | 236 |
| | II | 283.6 | 0.405 | -27.2 | 2.5 | $^4E$ ($\rightarrow {}^4T_3$) | DINYOO10 | 237 |
| **28** | | 302.7 | 0.329 | -11.5 | -10.6 | $^4T_5$ ($\rightarrow {}^4E$) | ZZZSTI01 | 238 |
| **29** | | 129.3 | 0.280 | 6.8 | 12.6 | $^5T_4$ ($\rightarrow {}^5E$) | KSCOSF | 239 |
| **30** | | 188.1 | 0.282 | -21.1 | 31.5 | $E_0$ ($\rightarrow {}^2T_0$) | IPASUC | 240 |
| **31** | | 287.8 | 0.367 | -22.0 | -0.8 | $^4E$ | KOJBOA | 241 |
| **32** | A | 253.2 | 0.348 | -34.6 | 22.0 | $E_3$ | –[f,g] | 242 |
| | B | 276.8 | 0.423 | -31.9 | 8.4 | $^4T_3$ ($\rightarrow {}^4E$) | | |
| **33** | | 117.9 | 0.319 | 14.3 | 7.3 | $^5T_4$ ($\rightarrow E_4$) | SAFZII | 243 |
| **34** | | 303.7 | 0.317 | -10.8 | -10.5 | $^4T_5$ ($\rightarrow {}^4E$) | KANJOY | 244 |
| **35** | | 259.7 | 0.340 | -31.8 | 17.3 | $E_3$ ($\rightarrow {}^4T_3$) | IMATUL | 245 |
| **36** | | 251.8 | 0.456 | 45.0 | 29.4 | $E_3$ | BOBKUY10 | 246 |
| **37** | | 258.1 | 0.361 | -34.6 | 19.6 | $E_3$ ($\rightarrow {}^4T_3$) | –[g] | 247 |
| **38** | I[h] | 257.7 | 0.388 | -29.6 | 8.6 | $^4T_3$ ($\rightarrow {}^4E$) | MELEZT01 | 248 |
| | II[h] | 251.5 | 0.377 | -37.6 | 24.5 | $E_3$ | MELEZT02 | 249 |
| **39** | | 265.7 | 0.388 | -34.6 | 15.9 | $^4T_3$ ($\rightarrow E_3$) | PLANTE10 | 250 |
| **40** | A | 100.6 | 0.298 | 21.1 | -3.7 | $E_4$ ($\rightarrow {}^3T_4$) | KESTOS[e] | 251 |
| | B | 254.4 | 0.416 | -40.7 | 24.9 | $E_3$ ($\rightarrow {}^4T_3$) | | |
| **41** | A | 272.9 | 0.422 | -34.1 | 11.6 | $^4T_3$ ($\rightarrow {}^4E$) | CELGIJ[e] | 252 |
| | B | 252.3 | 0.348 | -34.6 | 22.2 | $E_3$ | | |
| **42** | A | 269.5 | 0.368 | -30.8 | 12.5 | $^4T_3$ | –[g] | 202,253 |
| | B | 301.6 | 0.386 | -14.7 | -11.3 | $^4T_5$ ($\rightarrow {}^4E$) | | |
| | C | 259.0 | 0.420 | -40.5 | 22.3 | $E_3$ ($\rightarrow {}^4T_3$) | | |
| **43** | | 274.4 | 0.397 | -30.9 | 9.6 | $^4T_3$ ($\rightarrow {}^4E$) | RAFINO | 254 |
| **44** | I | 272.0 | 0.410 | -33.1 | 11.8 | $^4T_3$ ($\rightarrow {}^4E$) | STACHY10 | 255 |
| | II | 281.3 | 0.254 | -17.1 | 3.2 | $^4E$ ($\rightarrow {}^4T_3$) | STACHY01 | 256 |
| **45** | A | 261.7 | 0.416 | -37.9 | 19.7 | $^4T_3$ ($\rightarrow E_3$) | VIPRAN[e] | 257 |
| | B | 259.5 | 0.383 | -36.3 | 19.7 | $E_3$ ($\rightarrow {}^4T_3$) | | |
| **α-D-fructofuranosyl derivatives:** | | | | | | | | |
| **24** | α | 277.3 | 0.403 | -29.8 | 7.3 | $^4T_3$ ($\rightarrow {}^4E$) | BIVZAH | 234 |
| **46** | | 357.4 | 0.352 | 21.1 | -37.4 | $^0E$ ($\rightarrow {}^0T_5$) | KEMXOP | 258 |
| **47** | | 53.6 | 0.356 | 38.1 | -32.8 | $^3T_2$ | GEMYEC | 259 |
| **48** | | 31.9 | 0.372 | 37.1 | -40.4 | $E_2$ ($\rightarrow {}^0T_2$) | –[g] | 260 |
| **α-L-sorbofuranosyl derivatives:** | | | | | | | | |
| **49** | | 264.6 | 0.416 | -38.0 | 18.4 | $^4T_3$ ($\rightarrow E_3$) | DXSORF | 261 |
| **50** | | 128.0 | 0.367 | 9.7 | 14.9 | $^5T_4$ ($\rightarrow {}^5E$) | DIPKGA | 262 |
| **51** | | 138.1 | 0.324 | 3.1 | 18.6 | $^5E$ ($\rightarrow {}^5T_4$) | PHISOR | 263 |

a) puckering angle ϕ and amplitude *q* according to Fig. 5-2[122,123]. – b) ring torsion angles F (O-$C_2$-$C_3$-$C_4$) and Y ($C_3$-$C_2$-O-$C_5$). – c) the main conformation and the direction of distortion are given. – d) Cambridge crystallographic Ref-code[192]. – e) Different fructofuranose ring systems per molecule. – f) Two independent molecules. – g) Coordinates not yet contained in the data base. – h) Different crystal forms.

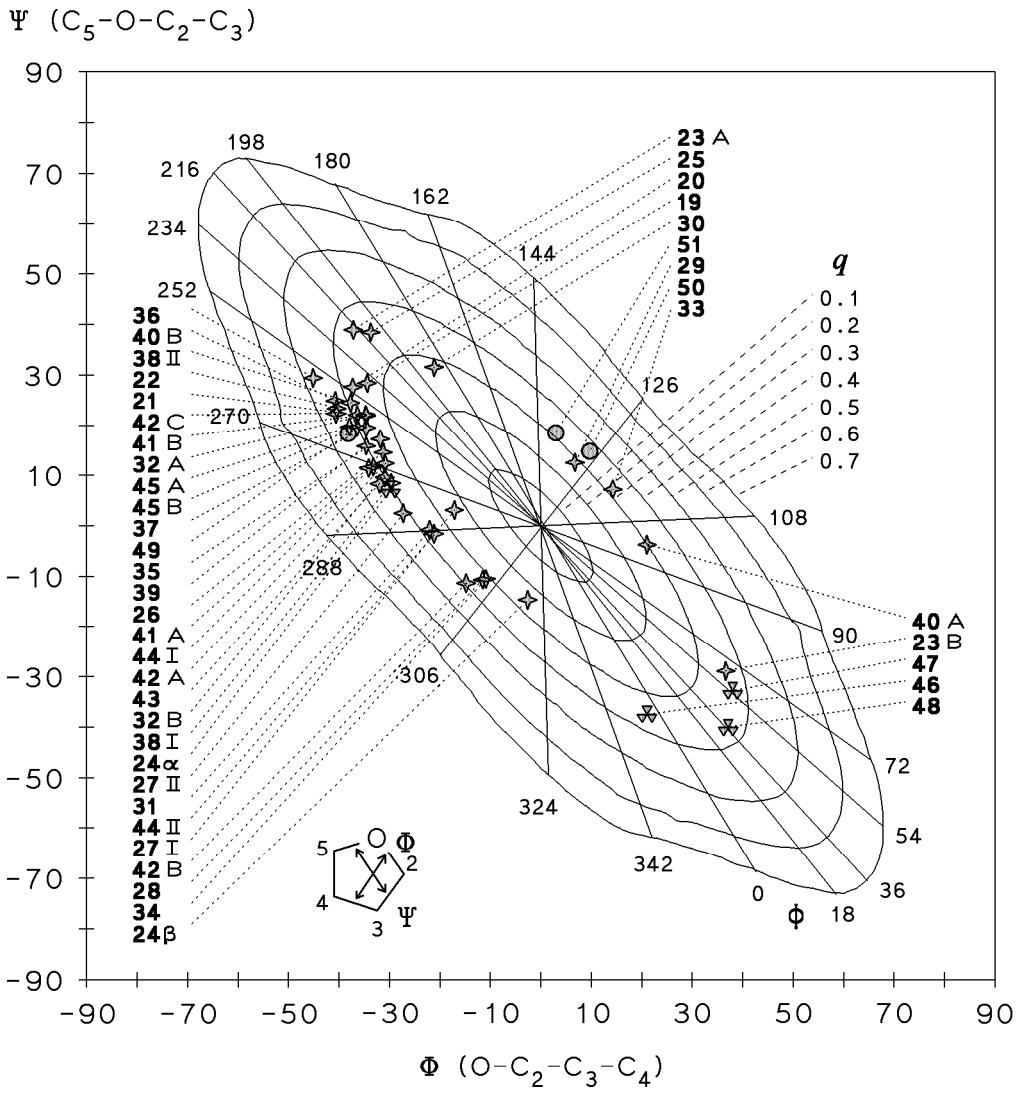


**Fig. 5-8.** Correlation of ring conformation (straight lines with the Cremer-Pople parameter ϕ as depicted in Fig. 5-2) and the Φ / Ψ-ring torsion angles as calculated for furanose rings ($r_{C\text{-}C} \approx 1.54$ Å, $r_{C\text{-}O} \approx 1.43$ Å). Contour plots of *q* indicate equal levels of ring distortion. The different asterisks and circles mark ring geometries of β-D-fructofuranosyl- (**19** – **45**), α-D-fructofuranosyl- (**24**α, **46** – **48**), and α-L-sorbofuranosyl-derivatives (**49** – **51**), respectively, as derived from crystal structural data (cf. Table 5-3 and 5-4, and Fig. 5-7).

Most notably, the data is in very good agreement with the asymmetrically extended energy contours within +15 kJ/mol, properly predicting the type (ϕ) and extent (*q*) of ring puckering even of constrained structures. Nevertheless, due to intramolecular constraints as well as crystal packing effects other conformations can become energetically available, e.g. the di-fructose-anhydride (**23**) exhibiting a $^{2}E$- as well as an unusual inverted $^{3}T_{2}$-ring geometry in two different β-furanose units, or sucrose octa-acetate (**28**) and octa-sulphate (**29**) adopting opposite $^{4}T_{5}$- and $^{5}T_{4}$-conformations (cf. Table 5-4).

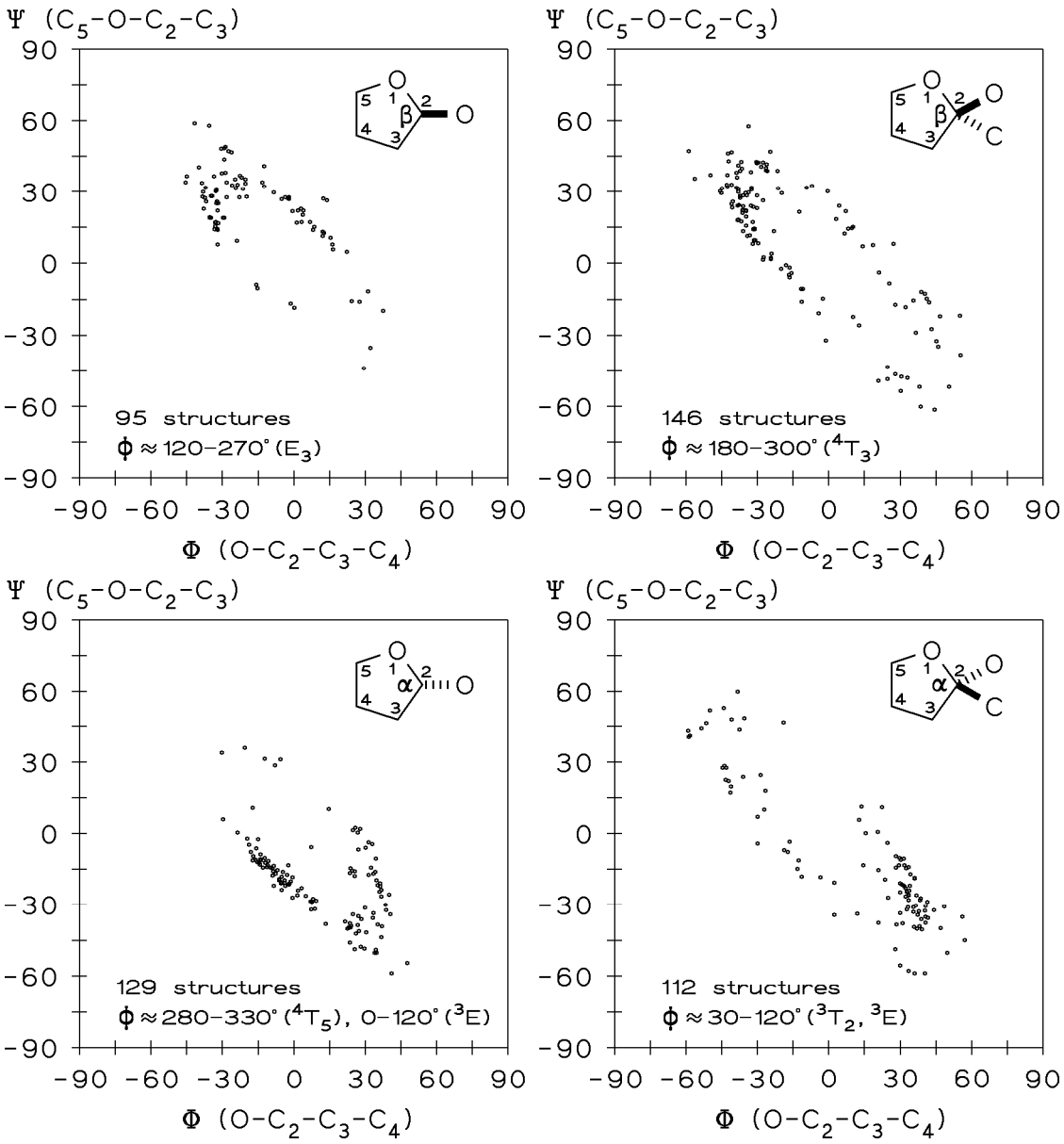


**Fig. 5-9.** Scatter plot of the solid state conformations[192] of β- (*upper row*) and α-furanose (*lower row*) ring systems (*left* hand side without, *right* side with an additional $C_2$-carbon substituent, respectively). As clearly evident, β- and α-furanoses do have opposite ring conformations, which also depend on the presence of further substituents on the $C_2$-anomeric center. The number of structures and typical conformations found – including the approx. Cremer-Pople puckering parameter ϕ – are given in addition.

Compared to the large data set on β-D-fructofuranoses, very little information is available for the α-derivatives. In the α-portion, the di-fructose-anhydride (**24**) shows a $^4T_3$-conformation, as typically observed in the β-series. In addition, $^0E$- and $^3T_2$-ring geometries (compounds **46** and **47**) have been observed. Most notably, the $E_2$-solid state conformation of penta-*O*-acetyl-α-D-fructofuranose (**48**) must be considered as

the best model for the unsubstituted α-D-fructofuranose. Again, the crystal structure data ($\phi \approx 355 - 55°$ and $q \approx 0.30 - 0.40$) is well in accord with the computational results presented above (Fig. 5-6), providing substantial evidence for distinctively different conformational properties of both fructofuranoses in relation to their anomeric configuration.

However, the anomeric effect[193] and the axial arrangement of the 2-OH group are not solely responsible for the observed conformational preferences of compounds of this type. A more far-reaching statistical crystal structure analysis of furanose ring systems also revealed the role of an additional carbon-substituent in 2-position as a factor determining the ring conformation (Fig. 5-9): in the β-series* the mean conformation is shifted from $^2T_3 \leftrightarrow E_3$ towards $E_3 \leftrightarrow {}^4T_3$ by additional C-2 substitution. In the case of unsubstituted α-compounds* $^4T_5$ and $E_2 \leftrightarrow {}^3T_2 \leftrightarrow {}^3E$-geometries are favored, the latter becoming even more probable by carbon extension in the 2-position. Obviously, not only the electronic effect of a pseudoaxial oriented anomeric oxygen substituent, but also the steric properties of an additional substituent in the more advantageous pseudoequatorial position govern the ring geometry of the fructofuranoses. The statistical scatter plots of Fig. 5-9 on the right side each correspond closely to the location as well as the asymmetric extension of the energy minima of the fructofuranose energy potential surfaces (Fig. 5-5 and 5-6), providing further evidence for the relevance of the computational results.

Due to the immense biological importance of furanoses as constituent components of DNA and RNA, it deems appropriate to note that the conformational trends manifested for the *O*-furanosides are not transferable to their nitrogen analogs. NMR-experimental[265], statistical solid state structure analysis[199,266,267] and computational studies[200,264,265,268] provide evidence for some conformational flexibility of the furanose in nucleic acids. In solid structures of *N*-furanosides (Fig. 5-10) two different main conformations of approx. $E_2 \leftrightarrow {}^3T_2 \leftrightarrow {}^3E \leftrightarrow {}^3T_4$ ($\phi \approx 20 - 100°$) and $^4T_3 \leftrightarrow {}^4E \leftrightarrow {}^4T_5$ ($\phi \approx 270 - 300°$) geometries** (puckering amplitudes $q \approx 0.25 - 0.55$) are observed, the former being characteristic for B-DNA, the latter for A-type structures[269]. Low energy barriers of $5 - 17\,\mathrm{kJ/mol}$ allow for interconversion, but prevent free pseudorotation[268].

---

* The β- and α-labels used here refer to the ring-top and bottom-sides and the configuration of the anomeric center only, irrespective of the presence of further ring substituents, they are not related to carbohydrate nomenclature.

** In terms of correct IUPAC-recommended nomenclature of riboses this corresponds to $^2E$- and $^3E$-ring conformations.

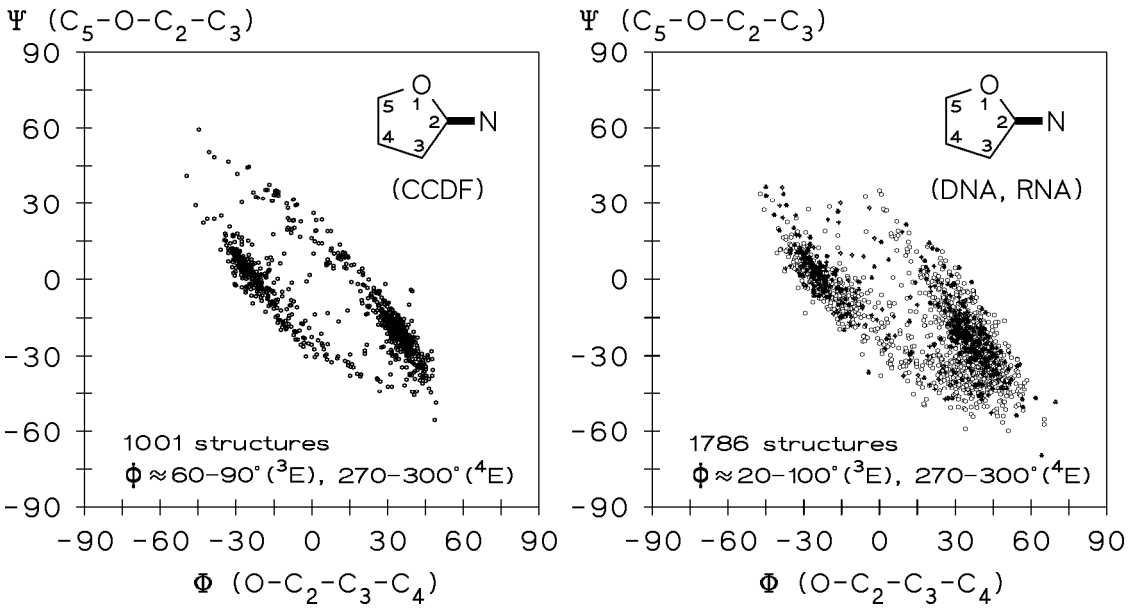


**Fig. 5-10.** Scatter plot of the Φ / Ψ-torsion angles as derived from solid state conformations of *N*-substituted furanoses (mainly β-nucleosides: *left* side CCDF[192]-structures, *right* side DNA- and RNA-structures[270]). The observed $^{3}$E- and $^{4}$E-main conformations (ribose nomenclature: $^{2}$E and $^{3}$E) differ substantially from those adopted by *O*-furanoses.

Obviously, steric repulsions overcome the weaker anomeric effect of nitrogen substituents as compared to *O*-derivatives[193], leading to substantially altered conformational principles. In conclusion, the conformational preferences of furanoses are not an intrinsic property of the ring system itself[271], but depend to a major extent on the substitution pattern.

*NMR-Data in Relation to Molecular Conformation*

The *in vacuo* force-field calculations are supported by the solid state properties of furanose-derivatives. However, the molecular conformation in solution might differ therefrom to some extent, such that it was necessary to counter-check the calculated data with the information available from NMR-experimental results.

The Karplus-type[272] H-C-C-H-torsion angle dependency of coupling constants leads to a correlation of the $^{3}J_{H\text{-}H}$-values with different ring conformations. In Fig. 5-11, the relationship between H-H-torsions angles and the ring puckering parameters as calculated for idealized furanose ring geometries is shown as a three-dimensional orthogonal plot $\phi_{H\text{-}H} = f(\phi, q)$. The $\phi_{H\text{-}H}$-values are directly related to the ring torsion angles around the central carbon-carbon bond. Their relationship to the puckering angle $\phi$ at constant puckering amplitudes $q$ can be described by a shifted cosine-function, the – at least in the first approximation – linear dependency from

the puckering amplitude leads to $\phi_{H\text{-}H}(\phi, q) = A + B\,q\cos(\phi + C)$ as a mathematical descriptor for the correlation in medium-distorted rings (cf. Table 5-5), where the parameter $A$ corresponds to the equilibrium torsion angle for a flat five-membered ring.

In contrast to earlier Dreiding-type model based estimations of H-H-torsion angles and $^3J$-values for maximal puckered furanose ring systems only[273], the computed exact $H_3$-$C_3$-$C_4$-$H_4$- ($\phi_{3,4} \rightarrow J_{3\text{-}H,4\text{-}H}$) and $H_4$-$C_4$-$C_5$-$H_5$-torsions ($\phi_{4,5} \rightarrow J_{4\text{-}H,5\text{-}H}$) yield a quantitative relationship between coupling constants and the Cremer-Pople-parameters $\phi$ and $q$, including the electronegativity effect of the substitution pattern[274] by use of the generalized Haasnoot-equation[275]. The contour-type correlation presented in Fig. 5-11 applies equivalently to *O*-substituted and OH-free β- as well as α-D-fructofuranoses. The $J_{3,4}$- and $J_{4,5}$-contours are rotated by approx. 36 degrees in $\phi$ relative to each other, as ideally expected for ring geometries with equal bond lengths. The unequal offsets for $J_{3,4}$ and $J_{4,5}$ for a flat ring ($q = 0.0$) originate from differences in the substitution pattern and stereochemistry at $C_3$-$C_5$.

The experimentally observed $^1$H-$^1$H-ring coupling constants for a large number of β- and α-D-fructofuranose derivatives are summarized in Table 5-6 and 5-7[37,194,196,273,276-282], as well as the data for some *spiro*-anellated fructose derivatives (Table 5-8)[235,283], and some fructofuranose containing unprotected saccharides (Table 5-9)[39,284-287]. Despite the fact, that the coupling constants cover a large range of values in both cases, clear-cut differences can be observed: in the α-series both coupling constants – most notably $J_{3,4}$ – are almost invariably lower ($J_{3,4} \approx 1 - 3$ Hz, $J_{4,5} \approx 4 - 6$ Hz) than those measured for the β-compounds ($J_{3,4} \approx J_{4,5} \approx 5 - 7$ Hz and $J_{3,4} \approx J_{4,5} \approx 7.5 - 8.5$ Hz for unprotected saccharides), and no significant overlap of the data ranges can be observed.

The best-fit virtual solution conformations of the β-D-fructofuranoses calculated from the coupling constants according to the correlation of Fig. 5-11 are centered around the $^2\text{E} \leftrightarrow {}^2\text{T}_3 \leftrightarrow \text{E}_3$ sector of the pseudorotational pathway (Table 5-6, mean values and standard deviations of $\phi \approx 240 \pm 10°$ and $q \approx 0.36 \pm 0.06$). It is noteworthy that the very uniform geometries and the reasonable $q$-values – as compared to the experimental and calculated data of the model compounds described above (Table 5-2) – strongly attest towards substantially restricted pseudorotation of β-furanoses and their distinctive conformational preferences.

An entirely different situation is computed within the α-series, where $^0\text{T}_5 \leftrightarrow {}^0\text{E} \leftrightarrow {}^0\text{T}_2$ conformations ($\phi \approx 350 \pm 20°$ and $q \approx 0.15 \pm 0.05$) are preferred[281], whereas the puckering amplitudes are obviously underestimated (Table 5-7).

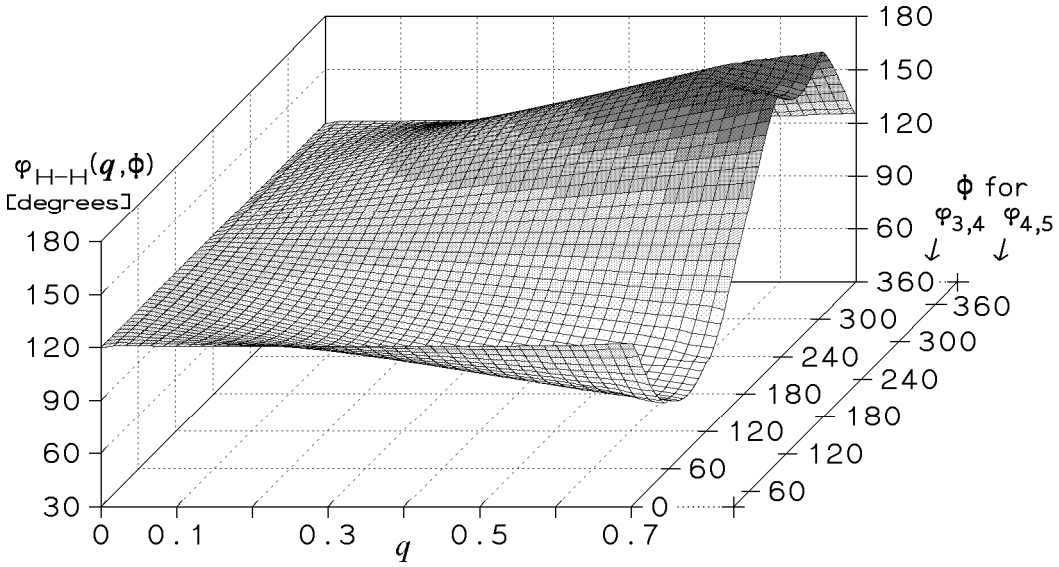


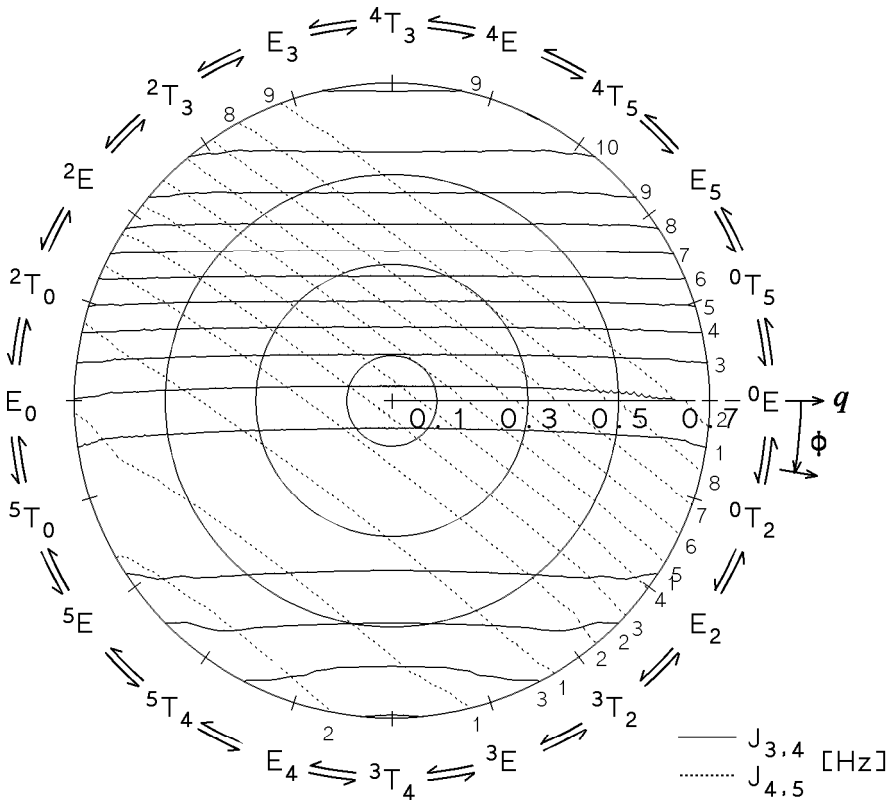


**Table 5-5.** Approximation of $^{1}$H-$^{1}$H-torsion angles as a function of ring puckering parameters in the range of $\phi = 0 – 360°$ and $q = 0.15 – 0.55$, and calculated root mean square deviations from exact values.

| $\varphi_{H\text{-}H}(\phi,q) = A + Bq\cos(\phi + C)$ torsion angle | parameters [°] $A$ | $B$ | $C$ | RMS-deviation |
|---|---|---|---|---|
| $\varphi_{3\text{-}H,4\text{-}H}$ | 122.1 | 98.3 | 90.0 | ±0.79° |
| $\varphi_{4\text{-}H,5\text{-}H}$ | -122.7 | -102.9 | 52.9 | ±0.80° |

**Fig. 5-11.** Orthogonal 3D-plot of the relationship between absolute values of H-H-torsion angles (|φ|) and ring puckering parameters (ϕ and *q*, *left* side) for fructofuranoses, and polar coordinate contour plot of the correlation of calculated $^{3}J_{3\text{-}H,4\text{-}H}$ (solid lines) and $^{3}J_{4\text{-}H,5\text{-}H}$ (dashed lines) $^{1}$H-$^{1}$H-coupling constants (in Hz, *right* side) with ϕ and *q* derived therefrom.

**Table 5-6.** $^1$H-$^1$H-coupling constants (mainly in $CDCl_3$) and corresponding best-fit virtual solution conformations of β-D-fructofuranosides.

| compound | | $R^1$ | $R^2$ | $R^3$ | coupling $^3J_{3,4}$ | coupling $^3J_{4,5}$ | Cremer-Pople-Par.[a] $\phi$ | Cremer-Pople-Par.[a] $q$ | virtual conformation[b] | ref. |
|---|---|---|---|---|---|---|---|---|---|---|
| 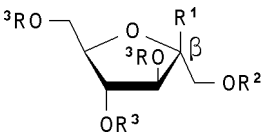 | **52** | OMe | H | H | 8.2 | 7.5 | 254 | 0.41 | $E_3$ | 37 |
| | **53** | OMe | TMS | TMS | 5.5 | 5.5 | 245 | 0.26 | $E_3$ ($\rightarrow {}^2T_3$) | 273 |
| | **54** | OMe | Ac | Ac | 7.0 | 5.0 | 229 | 0.43 | $^2T_3$ ($\rightarrow {}^2E$) | 276 |
| | **55** | -OC(CH$_3$)$_2$- | | Ac | 6.5 | 4.5 | 226 | 0.40 | $^2T_3$ ($\rightarrow {}^2E$) | 277 |
| | **56** | -OC(CH$_3$)$_2$- | | Bn | 3.9 | 5.9 | 287 | 0.16 | $^4E$ | 278 |
| | **57** | -O(CO)- | | Bn | 6.9 | 5.7 | 239 | 0.37 | $^2T_3$ ($\rightarrow E_3$) | 278 |
| | **58** | OH | OH | Bn | 6.5 | 6.2 | 249 | 0.32 | $E_3$ | 278 |
| | **59** | OH | Ac | Bn | 4.9 | 8.9 | 327 | 0.40 | $E_5$ ($\rightarrow {}^0T_5$) | 278 |
| | **60** | OH | Bz | Bn | 4.6 | 9.2 | 331 | 0.45 | $E_5$ ($\rightarrow {}^0T_5$) | 278 |
| | **61** | OH | Bz | Bz | 5.8 | 4.4 | 226 | 0.35 | $^2T_3$ ($\rightarrow {}^2E$) | 194 |
| | **62** | OMe | Bz | Bz | 6.9 | 5.6 | 238 | 0.37 | $^2T_3$ ($\rightarrow E_3$) | 279 |
| | **63** | OAc | Bz | Bz | 5.6 | 5.4 | 242 | 0.28 | $^2T_3$ ($\rightarrow E_3$) | 279 |
| **52 – 69** | **64** | $N_3$ | Bz | Bz | 5.7 | 5.5 | 243 | 0.28 | $E_3$ ($\rightarrow {}^2T_3$) | 279 |
| | **65** | SePh | Bz | Bz | 2.6 | 6.0 | 335 | 0.18 | $^0T_5$ ($\rightarrow E_5$) | 279 |
| | **66** | OMe | Bn | Bz | 1.3 | 5.0 | 8 | 0.20 | $^0E$ ($\rightarrow {}^0T_2$) | 196 |
| | **67** | OEt | Bn | Bn | 7.0 | 7.0 | 258 | 0.33 | $E_3$ ($\rightarrow {}^4T_3$) | 280 |
| | **68** | OH | Bn | Bn | 5.2 | 5.0 | 238 | 0.26 | $^2T_3$ ($\rightarrow E_3$) | 278 |
| | **69** | OH | Piv | Piv | 5.2 | 4.4 | 228 | 0.30 | $^2T_3$ ($\rightarrow {}^2E$) | 194 |
| 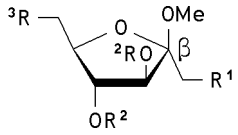 | **70** | H | Ac | OAc | 7.1 | 5.5 | 235 | 0.40 | $^2T_3$ | 281 |
| | **71** | OAc | Ac | H | 6.9 | 5.6 | 237 | 0.37 | $^2T_3$ ($\rightarrow E_3$) | 281 |
| | **72** | F | Ac | F | 7.3 | 7.1 | 257 | 0.35 | $E_3$ ($\rightarrow {}^4T_3$) | 281 |
| | **73** | Cl | Ac | OAc | 7.2 | 5.3 | 232 | 0.42 | $^2T_3$ | 281 |
| | **74** | OAc | Ac | Cl | 6.6 | 5.3 | 235 | 0.37 | $^2T_3$ | 281 |
| | **75** | Cl | Ac | Cl | 7.0 | 5.8 | 240 | 0.37 | $^2T_3$ ($\rightarrow E_3$) | 281 |
| | **76** | $N_3$ | Ac | OAc | 6.9 | 5.6 | 238 | 0.37 | $^2T_3$ ($\rightarrow E_3$) | 281 |
| | **77** | NHAc | Ac | OAc | 5.5 | 5.1 | 238 | 0.28 | $^2T_3$ ($\rightarrow E_3$) | 281 |
| **70 – 78** | **78** | F | Bz | OBz | 6.5 | 5.5 | 238 | 0.35 | $^2T_3$ ($\rightarrow E_3$) | 281 |

a) puckering angle $\phi$ and amplitude $q$ according to Fig. 5-2[122,123]. – b) the main conformation and the direction of distortion are given.

NMR-parameter derived geometry considerations might lead to virtual conformations without any physical relevance[288] if conformational averaging is fast on the NMR-time scale, thus limiting the applicability of this method in the case of flexible molecules. Obviously, the clear correlation between the coupling constants and the anomeric configuration of fructofuranoses (the Haasnoot-type derived coupling constants do not depend on the stereogeometry at the anomeric center!) must be interpreted as an indication for substantially hindered pseudorotation and significantly different ring geometries in both the β- and the α-case. However, if time-averaging is nevertheless important, it must be considered to occur especially in the very shallow contour region of $J_{3,4} \approx 0 - 2$ Hz, thus extending the conformational space available for the α-D-fructofuranoses along the $J_{4,5}$ iso-contour lines towards the $E_2 \leftrightarrow {}^3T_2 \leftrightarrow {}^3E$-region, and, simultaneously towards higher puckering amplitudes $q$.

**Table 5-7.** $^1$H-$^1$H-coupling constants (mainly in $CDCl_3$) and corresponding best-fit virtual solution conformations of α-d-fructofuranosides.

| compound | | $R^1$ | $R^2$ | $R^3$ | coupling $^3J_{3,4}$ | coupling $^3J_{4,5}$ | Cremer-Pople-Par.[a] $\phi$ | Cremer-Pople-Par.[a] $q$ | virtual conformation[b] | ref. |
|---|---|---|---|---|---|---|---|---|---|---|
| 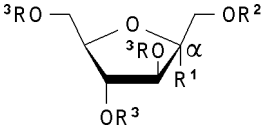 | **79** | OMe | H | H | 3.2 | 6.0 | 313 | 0.16 | $^4T_5$ ($\rightarrow$ $E_5$) | 37 |
| | **80** | OMe | Ac | Ac | 2.0 | 5.0 | 345 | 0.12 | $^0T_5$ ($\rightarrow$ $^0E$) | 276 |
| | **81** | OAc | Ac | Ac | 4.0 | 6.0 | 288 | 0.17 | $^4E$ | 282 |
| | **82** | F | Ac | Ac | 1.0 | 5.0 | 14 | 0.25 | $^0T_2$ ($\rightarrow$ $^0E$) | 282 |
| | **83** | OAc | Bn | Bz | 1.3 | 4.2 | 13 | 0.12 | $^0T_2$ ($\rightarrow$ $^0E$) | 196 |
| | **84** | OBz | Bn | Bz | 1.8 | 4.1 | 342 | 0.05 | $^0T_5$ | 196 |
| | **85** | OEt | Bn | Bn | 2.5 | 6.0 | 332 | 0.17 | $E_5$ ($\rightarrow$ $^0T_5$) | 280 |
| | **86** | OMe | Bn | Bz | 1.5 | 4.9 | 0 | 0.15 | $^0E$ | 196 |
| | **87** | H | Bz | Bz | 1.2 | 3.6 | 29 | 0.07 | $E_2$ ($\rightarrow$ $^0T_2$) | 279 |
| | **88** | OH | Bz | Bz | 1.7 | 4.6 | 356 | 0.11 | $^0E$ ($\rightarrow$ $^0T_5$) | 194,196 |
| | **89** | OMe | Bz | Bz | 1.5 | 5.0 | 0 | 0.17 | $^0E$ | 279 |
| | **90** | O*i*Pr | Bz | Bz | 1.5 | 4.5 | 1 | 0.11 | $^0E$ | 279 |
| | **91** | O*t*Bu | Bz | Bz | 1.5 | 4.5 | 1 | 0.11 | $^0E$ | 279 |
| | **92** | OAc | Bz | Bz | 2.9 | 5.5 | 313 | 0.12 | $^4T_5$ ($\rightarrow$ $E_5$) | 279 |
| | **48** | OBz | Bz | Bz | 2.2 | 4.7 | 319 | 0.08 | $E_5$ ($\rightarrow$ $^4T_5$) | 196,279 |
| | **93** | $N_3$ | Bz | Bz | 1.5 | 4.2 | 1 | 0.08 | $^0E$ | 279 |
| | **94** | SePh | Bz | Bz | 2.6 | 6.2 | 337 | 0.19 | $^0T_5$ ($\rightarrow$ $E_5$) | 279 |
| | **95** | OAc | Tos | Bz | 2.8 | 5.2 | 300 | 0.11 | $^4T_5$ ($\rightarrow$ $^4E$) | 196 |
| | **96** | OBz | Tos | Bz | 1.8 | 4.1 | 331 | 0.04 | $E_5$ ($\rightarrow$ $^0T_5$) | 196 |
| | **97** | OBz | All | Bz | 2.0 | 4.5 | 330 | 0.07 | $E_5$ ($\rightarrow$ $^0T_5$) | 196 |
| | **98** | OH | Piv | Piv | 2.2 | 5.2 | 337 | 0.13 | $^0T_5$ ($\rightarrow$ $E_5$) | 194 |
| | **99** | -OC(CH$_3$)$_2$- | | Bn | 2.7 | 4.6 | 279 | 0.08 | $^4E$ ($\rightarrow$ $^4T_3$) | 278 |
| | **100** | -O(CO)- | | Bn | 2.3 | 4.7 | 318 | 0.08 | $E_5$ ($\rightarrow$ $^4T_5$) | 278 |
| | **101** | OH | Ac | Bn | 1.7 | 3.2 | 196 | 0.05 | $^2T_0$ | 278 |
| | **102** | OH | Bz | Bn | 1.8 | 3.3 | 202 | 0.04 | $^2T_0$ ($\rightarrow$ $^2E$) | 278 |
| | **103** | OH | Bn | Bn | 2.0 | 3.9 | 280 | 0.04 | $^4E$ ($\rightarrow$ $^4T_3$) | 278 |
| **48**, **79** – **103** | | | | | | | | | | |
| 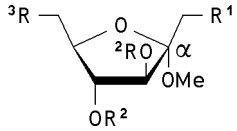 | **104** | H | Ac | OAc | 1.9 | 5.8 | 353 | 0.21 | $^0E$ ($\rightarrow$ $^0T_5$) | 281 |
| | **105** | OAc | Ac | H | 2.4 | 6.0 | 338 | 0.18 | $^0T_5$ ($\rightarrow$ $E_5$) | 281 |
| | **106** | F | Ac | F | 2.2 | 6.4 | 344 | 0.23 | $^0T_5$ | 281 |
| | **107** | Cl | Ac | OAc | 1.5 | 5.0 | 0 | 0.17 | $^0E$ | 281 |
| | **108** | OAc | Ac | Cl | 1.6 | 5.3 | 2 | 0.19 | $^0E$ | 281 |
| | **109** | Cl | Ac | Cl | 1.4 | 5.3 | 2 | 0.20 | $^0E$ | 281 |
| | **110** | $N_3$ | Ac | OAc | 2.2 | 5.3 | 337 | 0.13 | $^0T_5$ ($\rightarrow$ $E_5$) | 281 |
| | **111** | F | Bz | OBz | 2.2 | 4.9 | 325 | 0.09 | $E_5$ | 281 |
| **104** – **111** | | | | | | | | | | |

a) puckering angle $\phi$ and amplitude $q$ according to Fig. 5-2[122,123]. – b) the main conformation and the direction of distortion are given.

The conformational trends manifested for those simple fructofuranose derivatives are continued in a number of more complex *spiro*-1,3-dioxane anellated compounds (Table 5-8)[235,283]. In all cases, the β-configuration leads to $^2T_3$-conformations (**25**, **112** – **118**), the solution conformation of **25** ($^2T_3$) even resembles closely to its solid state X-ray structure ($^2E \rightarrow {}^2T_0$, cf. Table 5-4).

The opposite behavior is observed for the α-compound **119**[235], exhibiting an inverted $E_2$-ring structure. This may be interpreted as a hint for the relevant extension of the conformational space towards the $E_2 \leftrightarrow {}^3T_2$-region of α-fructofuranoses proposed above: increasing molecular rigidity by *spiro*-anellation leads to lowered time-averaging of the coupling constants, and, in consequence, to a decrease of the measured $J_{3,4}$-value and higher calculated puckering amplitudes. In comparison to the α-D-fructofuranoses, for **119** a significantly increased value of $q \approx 0.49$ was computed for the best-fit virtual conformation for the NMR-parameters.

Most notably, the di-fructose anhydride (1',2-anhydro-[1-(α-D-fructofuranosyl)-β-D-fructofuranose], **120**) unifies a β- as well as an α-furanoid ring within one molecule in an almost symmetrical fashion, each of them being characterized by the typical $^2$E- and $^0$E-conformations, the experimental coupling constants being within the standard ranges, respectively.

**Table 5-8.** Conformations of *spiro*-fructofuranosides in relation to their $^1$H-$^1$H-coupling constants (300 MHz, $CDCl_3$).

| compound | | $R^1$ | coupling $^3J_{3,4}$ | coupling $^3J_{4,5}$ | Cremer-Pople-Par.[a] $\phi$ | Cremer-Pople-Par.[a] $q$ | virtual conformation[b] | ref. |
|---|---|---|---|---|---|---|---|---|
| 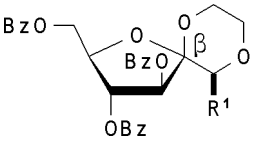 | **25** | OBz | 7.1 | 5.5 | 235 | 0.40 | $^2T_3$ | 235 |
| | **112** | OH | 5.1 | 3.9 | 221 | 0.33 | $^2E$ ($\rightarrow {}^2T_3$) | 235 |
| | **113** | Br | 6.5 | 5.4 | 237 | 0.35 | $^2T_3$ ($\rightarrow E_3$) | 235 |
| 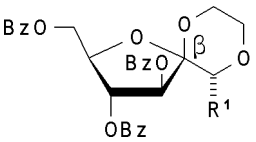 | **114** | OH | 5.9 | 4.4 | 226 | 0.36 | $^2T_3$ ($\rightarrow {}^2E$) | 235 |
| | **115** | OMe | 6.8 | 5.2 | 233 | 0.39 | $^2T_3$ | 235 |
| | **116** | O*i*Pr | 6.0 | 5.1 | 235 | 0.33 | $^2T_3$ | 235 |
| | **117** | $OC_6H_{11}$ | 5.6 | 5.1 | 237 | 0.29 | $^2T_3$ ($\rightarrow E_3$) | 235 |
| | **118** | OChol | 5.4 | 4.3 | 226 | 0.32 | $^2T_3$ ($\rightarrow {}^2E$) | 235 |
| 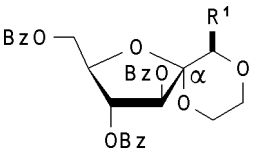 | **119** | OBz | 0.4 | 4.4 | 30 | 0.49 | $E_2$ ($\rightarrow {}^0T_2$) | 235 |
| 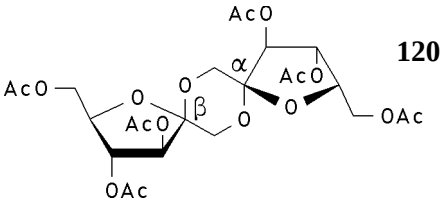 | **120** | β[c] | 6.5 | 4.3 | 224 | 0.42 | $^2E$ ($\rightarrow {}^2T_3$) | 283 |
| | | α[c] | 1.7 | 5.4 | 354 | 0.18 | $^0E$ ($\rightarrow {}^0T_5$) | 283 |

a) puckering angle $\phi$ and amplitude $q$ according to Fig. 5-2[122,123]. – b) the main conformation and the direction of distortion are given. – c) 100 MHz.

Biologically most important, the ring coupling constants in some β-D-fructofuranose containing saccharides[39,284-287] are even higher ($J_{3,4} \approx J_{4,5} \approx 7.5 - 8.5$ Hz) than those observed for the *O*-modified derivatives. Their calculated virtual solution conformations are almost identically located within the $E_3 \leftrightarrow {}^4T_3$-region of the pseudorotational wheel ($\phi \approx 264 \pm 5°$ and $q \approx 0.42 \pm 0.02$, Table 5-9). Even for ring A of 1-kestose (**40**), the unusual $E_4$ ($\rightarrow {}^3T_4$) conformation observed in the solid state, inverts during relaxation in solution, thus forming a more common $E_3 \leftrightarrow {}^4T_3 \leftrightarrow {}^4E$ geometry. The pronounced preference of $^4T_3$-ring conformations seems to be an equilibrium compromise between steric repulsions between O-2 and $CH_2$-6, the anomeric effect, and the tendency of the vicinal oxygen atoms 2-O, 3-O, and 4-O to favor *gauche*-relationships. For a series of aldopentose and aldohexose derived methyl furanosides the quasi-axial orientation of the methoxy substituent and the quasi-equatorial side chain has been deduced by calculation of molar optical rotations in combination with NMR-results[289], the reported $^3T_2$-conformations of the β-aldofuranosides are equivalent to predominating $^4T_3$-fructofuranose conformers. For methyl β-D-fructofuranoside itself, a $^4T_5 \leftrightarrow E_5$ geometry was proposed[41].

**Table 5-9.** Solution conformations of some fructofuranoside containing saccharides as derived from the respective $^1$H-$^1$H-coupling constants (in $D_2O$).

| compound | | coupling $^3J_{3,4}$ | coupling $^3J_{4,5}$ | Cremer-Pople-Par.[a] $\phi$ | Cremer-Pople-Par.[a] $q$ | virtual conformation[b] | ref. |
|---|---|---|---|---|---|---|---|
| Sucrose | **26** | 8.8 | 8.3 | 261 | 0.44 | $^4T_3$ ($\rightarrow E_3$) | 39 |
| 2-Deoxy-sucrose | **121** | 8.8 | 8.0 | 257 | 0.45 | $E_3$ ($\rightarrow {}^4T_3$) | 39 |
| 1-Kestose | **40** | 8.0 | 8.5 | 276 | 0.39 | $^4T_3$ ($\rightarrow {}^4E$) | 284, |
| | | 8.0 | 7.5 | 257 | 0.40 | $E_3$ ($\rightarrow {}^4T_3$) | 285 |
| Nystose | **42** | 8.73 | 8.64 | 269 | 0.43 | $^4T_3$ | 285, |
| | | 8.40 | 8.24 | 265 | 0.41 | $^4T_3$ ($\rightarrow E_3$) | 286 |
| | | 8.44 | 8.06 | 262 | 0.42 | $^4T_3$ ($\rightarrow E_3$) | |
| 1,1,1-Kestopentaose | **122** | 8.73 | 8.44 | 265 | 0.44 | $^4T_3$ ($\rightarrow E_3$) | 286 |
| | | 8.22 | 8.22 | 267 | 0.40 | $^4T_3$ ($\rightarrow E_3$) | |
| | | 8.36 | 7.78 | 258 | 0.42 | $E_3$ ($\rightarrow {}^4T_3$) | |
| | | 8.58 | 7.69 | 255 | 0.44 | $E_3$ ($\rightarrow {}^4T_3$) | |
| Melezitose | **38** | 7.6 | 8.0 | 270 | 0.36 | $^4T_3$ | 287 |
| Raffinose | **43** | 8.4 | 8.0 | 261 | 0.42 | $^4T_3$ ($\rightarrow E_3$) | 287 |

a) puckering angle $\phi$ and amplitude $q$ according to Fig. 5-2[122,123]. – b) the main conformation and the direction of distortion are given.

The distinctive conformational differences of the β- and α-D-fructofuranoses become particularly obvious from the polar-coordinate scatter-plot of the best-fit virtual conformations on the conformational wheel (Fig. 5-12). The few exceptions

from these findings reported (compounds **65**, **66**, and **81**, in particular) probably require a reassignment of the anomeric configuration.

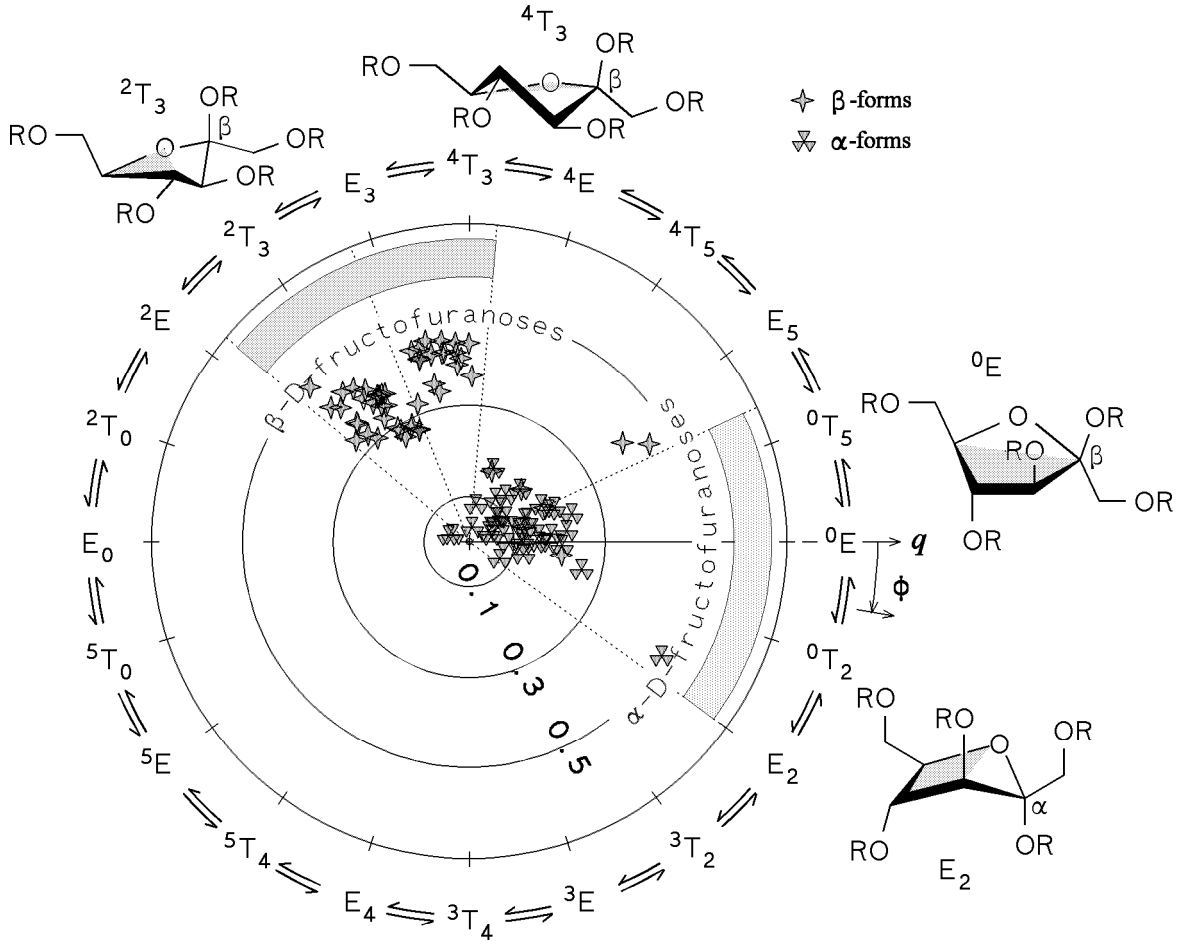


**Fig. 5-12.** Polar coordinate ($\phi$, $q$) scatter plot of the virtual conformations of fructofuranoses calculated from the $^3J_{3,4}$ and $^3J_{4,5}$ $^1$H-$^1$H-coupling constants. In the series of β-compounds the conformation varies from $^2T_3$ to $^4T_3$, while for α-derivatives mainly $E_2 \leftrightarrow {}^0T_2 \leftrightarrow {}^0E \leftrightarrow {}^0T_5$ conformations are observed. The formulas depicted in addition illustrate the approximate ring geometries including their main ring planes.

Previous computational studies of the flexibility of furanose rings completely neglect the influence of an anomeric substituent[271,290], or miss the 1-hydroxymethyl grouping[291]. Earlier molecular mechanics analysis of fructofuranose (MMP2[201] and MM3[202]) were interpreted in terms of considerable conformational freedom of the furanose ring. For β-D-fructofuranose, two local energy minima in the $E_3 \leftrightarrow {}^4T_3$ and the $^5T_4$ region were proposed[201], the former global minimum being consistent with the data reported here. Revision of the second minimum[202] revealed a more extended region centered around $E_4 \leftrightarrow {}^3T_4 \leftrightarrow E_3$. α-D-Fructofuranose was included in the MM2-study[201], the global minimum $^4E \leftrightarrow {}^4T_5 \leftrightarrow E_5$ and a higher energy $^3T_4 \leftrightarrow {}^3E$

structure differ considerably from the results presented here. Only the X-ray structure of **24**[234] was considered in this study as supportive evidence for the corresponding energy potential surface[201], no comparison with NMR-data was made. Now, on the basis of the calculatory data of this work (*vide supra*), the solid state conformation of **24** must be considered as non-typical for α-D-fructofuranose derivatives.

It has been noted that conformational analysis of furanoid rings based solely on interpretation of $^{1}$H-$^{1}$H-coupling constants might be tenuous, as long as additional support is not obtained by different methods, such as $^{1}$H-$^{13}$C-couplings[292]. In this report, the excellent conformity of combined computational and experimental techniques strongly attest towards the relevance of conformational parameters deduced from $^{1}$H-$^{1}$H-coupling constants.

In summary, the solution structures do not span an as large range of the conformational space as the crystal structures do, which might be attributed to the release of packing effects upon dissolution. In combination with the calculated energy potential surfaces of both D-fructofuranoses, the statistical crystal structure analysis and the interpretations of NMR-parameters strongly attest to considerably hindered pseudorotation of the furanose ring systems. All methods are consistent with each other and unequivocally predict opposite conformational properties for both different β- and α-anomers. The anomeric effect seems to be the strongest conformation determining force, being furthermore influenced by the presence of additional ring substituents, the 1-$CH_2OH$ group in particular. The accentuation of the anomeric effect by the tendency of bulky side chains to occupy pseudoequatorial positions had already been confirmed by experimental techniques for α- and β-D-*threo*-2-pentuloses[292] – configurationally similar to D-fructose, but missing the 6-$CH_2OH$ unit – as compared to D-*threo*-furanose[293,294] (missing both 1- and 6-$CH_2OH$ groups).

**Acyclic *keto*-D-Fructose**

In the equilibrium tautomeric mixture of fructose in solution, the acyclic *keto*-isomer is present to only very minute amounts of up to one percent. Therefore, exact NMR-data of this compound, by which information about preferred conformations could be obtained, is not available. From studies on the solid state structures of acyclic sugar chains[295] and glycosyl-alditols[296], as well as extensive $^{1}$H-[297-299] and $^{13}$C-NMR[300] investigations and molecular mechanics calculations[301], it is a well-established fact that polyols tend to favor a *gauche*-arrangement of 1,2-hydroxyl groupings in low-polar and protic solvents,

simultaneously avoiding energetically disadvantageous 1,3-diaxial like O-O- and C-O-repulsions[299].

A detailed NMR-study on D-*threo*-2-pentulose[292] – the configurational $C_5$-analog of *keto*-D-fructose – revealed both the OH-groups in the 1- and 3-position to adopt a *syn*-eclipsed conformation with the center carbonyl group. Assuming this geometry to be also retained in *keto*-D-fructose, all possible combinations of staggered conformations in respect to the $C_3$-$C_4$- and $C_4$-$C_5$-bonds leave only one rotamer that lacks unfavorable 1,5- or 1,6-repulsions (cf. Fig. 5-13). Obviously, this most stable conformer exhibits a (+)-*gauche* arrangement of O-3 and O-4, and a simultaneous $O_4$-$O_5$-*trans* disposition. In consequence, H-3 and H-4 must adopt a (–)-*gauche*, and H-4 / H-5 a *trans*-relationship.

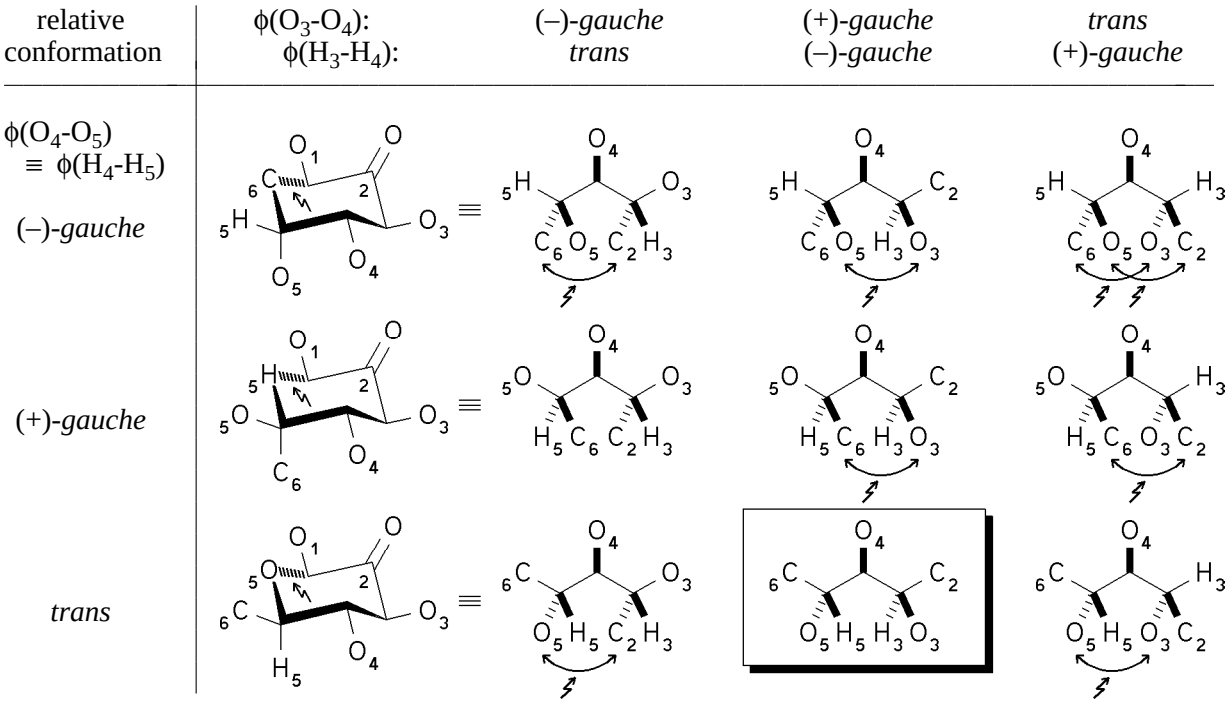


**Fig. 5-13.** In *keto*-D-fructose, all different combinations of staggered $C_3$-$C_4$- and $C_4$-$C_5$-conformations except the framed one lead to energetically unfavorable 1,5- (1,3-diaxial like) or 1,6-interactions (steric overlaps). Thus, the (+)-*gauche*-disposition of $O_3$-$O_4$ and the *trans*-arrangement of $O_4$-$O_5$ must be considered as the minimum energy rotamer.

Further corroboration for those predictions can be obtained from the $^1$H-$^1$H-NMR coupling patterns along the carbon chain of *keto*-D-fructose (**123** – **128**) and 6-chloro-6-deoxy-*keto*-D-fructose (**129**, **130**) derivatives (Table 5-10)[196,302]: the unusually large $J_{1A,1B}$-coupling (≈ 17 – 18 Hz) can be attributed to a symmetrical *syn*-eclipsed

orientation of the $CH_2OH$-group in respect to the carbonyl group[292,303]. By comparison of the experimental data with values calculated for different H-H-torsion angles (Table 5-11), the small couplings $J_{3,4} \approx 1.9 - 2.4$ Hz indicate a (–)-*gauche* arrangement of H-3 and H-4 (calc. 0.75 Hz), and the rather large values for $J_{4,5} \approx 8.3 - 9.1$ Hz are consistent with a *trans*-structure of H-4 and H-5 (calc. 9.75 Hz).

**Table 5-10.** $^1$H-$^1$H-coupling constants (300 MHz, $CDCl_3$) of acyclic *keto*-d-fructose derivatives.

| compound | | $R^1$ | $R^2$ | $R^3$ | $^1$H-$^1$H-coupling constants [Hz] $\lvert J_{1A,1B} \rvert$ | $J_{3,4}$ | $J_{4,5}$ | $J_{5,6R}$ | $J_{5,6S}$ | ref. |
|---|---|---|---|---|---|---|---|---|---|---|
| 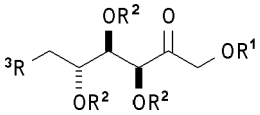 | **123** | Bz | Bz | OBz | 17.5 | 2.4 | 8.4 | 4.8 | 2.9 | 302 |
| | **124** | Me | Bz | OBz | 17.0 | 2.0 | 8.3 | 5.1 | 2.9 | 196 |
| | **125** | Me | Bz | OAc | 18.0 | 2.3 | 8.3 | 5.0 | 3.0 | 196 |
| | **126** | Bn | Bz | OAc | 17.1 | 1.9 | 8.6 | 4.7 | 2.8 | 196 |
| | **127** | All | Bz | OAc | 17.0 | 2.0 | 8.5 | 4.9 | 2.8 | 196 |
| | **128** | Ac | Ac | OAc | 17.4 | 2.2 | 9.1 | 4.8 | 3.3 | 302 |
| | **129** | Bz | Bz | Cl | 17.2 | 2.2 | 8.4 | 4.3 | 2.7 | 302 |
| | **130** | Ac | Ac | Cl | 17.3 | 2.0 | 9.0 | 5.5 | 3.3 | 302 |

**Table 5-11.** Calculated $^1$H-$^1$H-coupling constants for *O*-acylated *keto*-fructoses.

| $^1$H-$^1$H-coupling [Hz] | $H^{(n)}$-$H^{(n+1)}$-conformation (–)-*gauche* | *trans* | (+)-*gauche* |
|---|---|---|---|
| $J_{3\text{-H},4\text{-H}}$ | 0.75 | 9.85 | 4.25 |
| $J_{4\text{-H},5\text{-H}}$ | 2.51 | 9.75 | 2.49 |

| $^1$H-$^1$H-coupling [Hz] | $CH_2OH$-conformation* *gauche-gauche* | *gauche-trans* | *trans-gauche* |
|---|---|---|---|
| $J_{5\text{-H},6\text{-H}R}$ | 0.75 | 10.16 | 4.28 |
| $J_{5\text{-H},6\text{-H}S}$ | 2.50 | 2.53 | 10.16 |

* first torsion angle referring to $O_5$-$C_5$-$C_6$-$O_6$, second to $C_4$-$C_5$-$C_6$-$O_6$:

View $C_6 \rightarrow C_5$

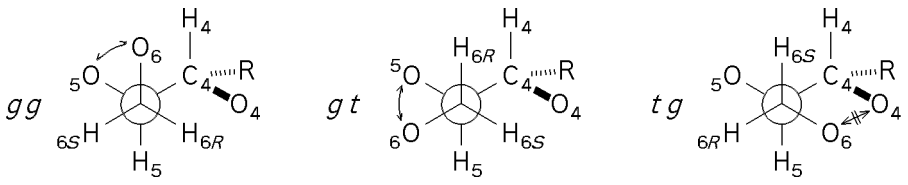

The theoretical considerations of Fig. 5-13 and the experimental data point towards the same rotamer as the global energy minimum structure. The small differences of approx. 1 Hz between calculated and observed couplings even indicate that in solution no significant conformational averaging by the presence of multiple structures of equal energy takes place. From the data of Table 5-11 and the measured coupling constants $J_{5,6R} \approx 5$ Hz and $J_{5,6S} \approx 3$ Hz (Table 5-10), the relative rotamer population of the hydroxymethyl group[102] can be estimated to be approx. *gg* : *gt* : *tg* = 47 : 47 : 6. Thus, O-5 and O-6 are correlated by a somehow flexible (±)-*gauche*-arrangement, the latter *tg* conformer being destabilized by 1,3-diaxial like interactions between O-4 and O-6. By force field based analysis a molecular model of *keto*-D-fructose was generated, to which these steric restrictions apply (Fig. 5-14): the all-*syn* arrangement of $C_1$-$O_1$-, $C_2$-$O_2$-, and $C_3$-$O_3$-bonds, and the polyol-structure inherent *gauche*-disposition of the hydroxyl groups OH-3 / OH-4 and OH-5 / OH-6 along the nearly undistorted, linear zigzag carbon-chain are clearly evident. The C-1 to C-6 backbone is even more extended by O-6 of the terminal hydroxymethyl group (*gt* rotamer), as usually observed for alditols in aqueous solutions[298].

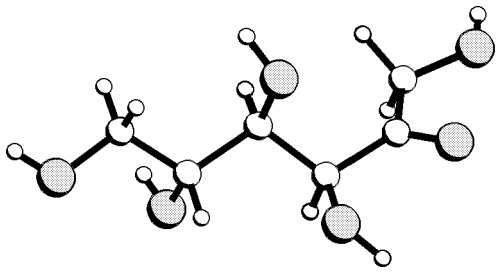

**Fig. 5-14.** Proposed low-energy conformation of *keto*-D-fructose.

Due to intramolecular hydrogen bonding effects which are not observed in alditol crystal structures[295] (and certainly are not relevant in aqueous solutions), the proposed structure is not the calculated global energy minimum geometry, but the most stable one without intramolecular H-bonds.

## Structure-Sweetness Relationships

Present structure-sweetness correlations[4,152-154] on the basis of the original Shallenberger / Kier concept[1-3] presume the existence of a common structural tripartite element in all sweet tasting molecules: a hydrogen bond donor (AH-unit), a neighbored hydrogen bond acceptor functionality (B-portion), and an additional hydrophobic binding "point" (X). Recent molecular modeling studies necessitated a modification of these ideas, thus that a whole extended molecular region, rather than a

specific binding point must be responsible for the hydrophobic interaction with the sweetness receptor[19] (this work, Chapter 2 and 3).

*Molecular Contact Surfaces*

So far, from the comprehensive study of the conformational properties of all fructose tautomers reasonable molecular models for each compound were obtained, which now can be entered into more detailed molecular modelings in order to gain further information on their relative sweetness characteristics. In Fig. 5-15, all five isomers of the tautomeric equilibrium mixture of fructose in solution are shown, including the MOLCAD-program[48] generated contact surfaces[46] (roughly equivalent to the solvent-accessible surface[47], i.e. "how water sees the molecule") in dotted form.

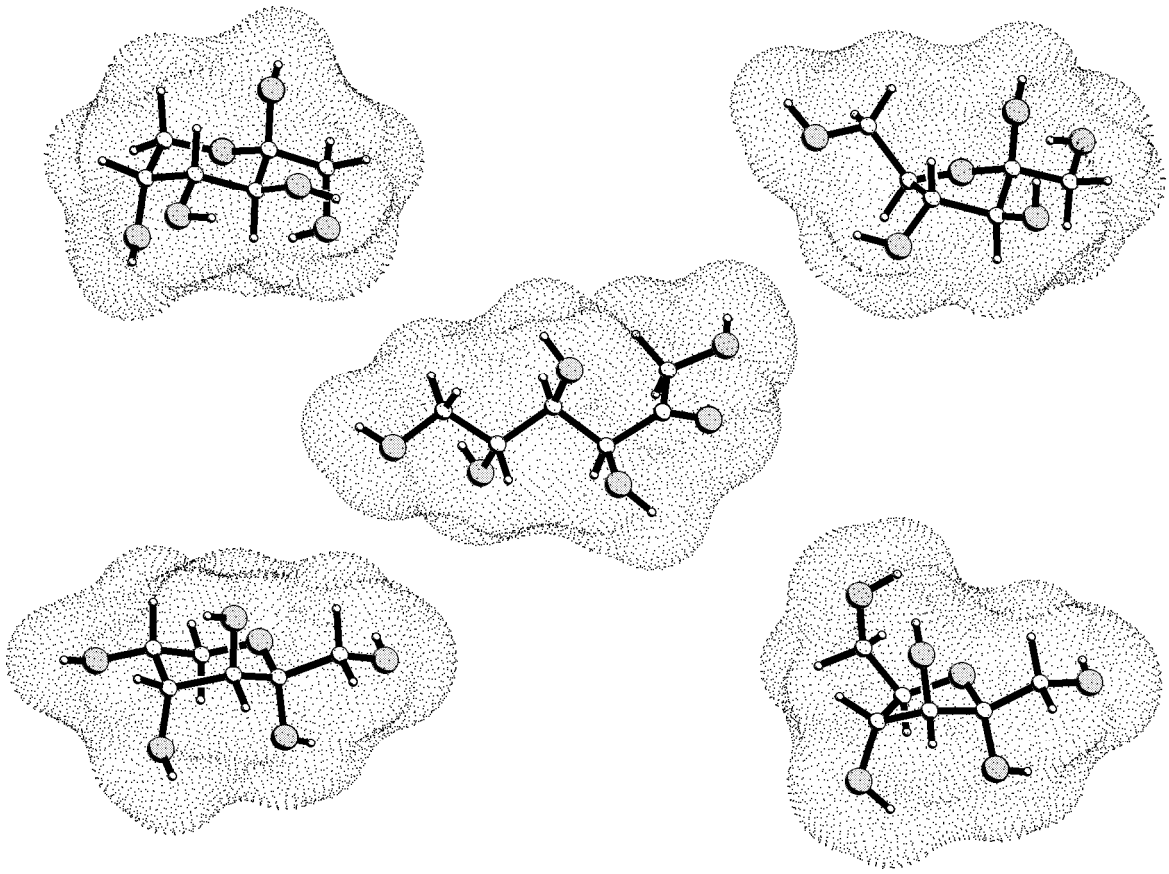

**Fig. 5-15.** Molecular low-energy geometries and dotted contact surfaces of all different fructose tautomers.

The molar volumes calculated from the molecular surfaces of the four cyclic isomers are of same magnitude of $^{\phi}V_{calc} = 180.8 \pm 0.8\,Å^3$ ( = $108.9 \pm 0.5\,cm^3/mol$), and thus agree well with the apparent molar volume of $^{\phi}V_{exp} = 105 - 111\,cm^3/mol$ ( = $175 - 184\,Å^3$) of D-fructose in equilibrated aqueous solutions obtained from

density measurements[101,134]. The excellent conformity of the experimental value of $^{\phi}V_{exp} = 108.5\,cm^3/mol$ for non-equilibrated solutions of β-D-fructopyranose at low concentrations[101] with the theoretical prediction of $108.4\,cm^3/mol$ for this isomer further indicates the relevance of molecular contact surfaces for the assessment of intermolecular interactions. The total surface area was computed to be $A_{tot} = 179 \pm 3\,Å^2$ in all cases except of the acyclic *keto*-form, for which slightly higher parameters ($^{\phi}V_{calc} = 113\,cm^3/mol$ and $A_{tot} = 192\,Å^2$) were estimated. In conclusion, at least the β-*p*-, β-*f*-, α-*f*-, and α-*p*-forms do have similar overall steric properties on the basis of which non of these isomers could be ruled out from structure-sweetness relationships.

*Molecular Lipophilicity Profiles*

The calculation of **m**olecular **l**ipophilicity (hydrophobicity) **p**atterns (**MLP**'s)[58] on molecular surfaces proved to represent a powerful tool for the assessment of relative sweetness potencies[19] (Chapter 2 and 3). In Fig. 5-16, the MLP's for the five different fructose tautomers mapped on the corresponding contact surfaces are shown, respectively. The color-code used here was adapted to the individual MLP range (private mapping) in each case. As clearly obvious from Fig. 5-17, the range of the individual MLP's (-0.093 < MLP < -0.028, in arbitrary units) is almost identical for the cyclic isomers, only the *keto*-form being more hydrophilic than the others.

In the β-*p*-form, the most hydrophobic surface area is extended all over the molecular "backside", comprising both the 6- and 1-$CH_2$ groups as well as the ring oxygen, the most hydrophilic region is made up by the 3- and 4-hydroxyl groups. The observed opposite side-distribution of hydrophobic and hydrophilic surface parts must be considered as a characteristic structural element of all sweeteners, in general the latter containing the hydrogen bonding AH-B-couple[19] (Chapter 2 and 3). Contrary to earlier suggestions[2,20,93,96-101,176,177] for D-fructose, which assign the AH-B-system of the sweetness triangle to the 1,2-diol grouping (in different orientations, respectively) and the hydrophobic X-part to the 6-methylene group only, it now becomes evident that the hydrophobic binding region of β-D-fructopyranose is made up by two dispersive centers, i.e. the 6-$CH_2$ as well as the 1-$CH_2$ groups. On the other side, the highly hydrophilic 3- and 4-OH groups most likely represent the AH-B-couple involved in hydrogen bonding with the sweetness receptor (cf. Chapter 4). These AH-B-assignments emerging from the MLP's support previous results of Birch *et al.*[101], who concluded from intensity-time studies of sweetness and structural similarities between glucose and fructose that the "anomeric center of D-fructose may play no direct role in the sweetness response".

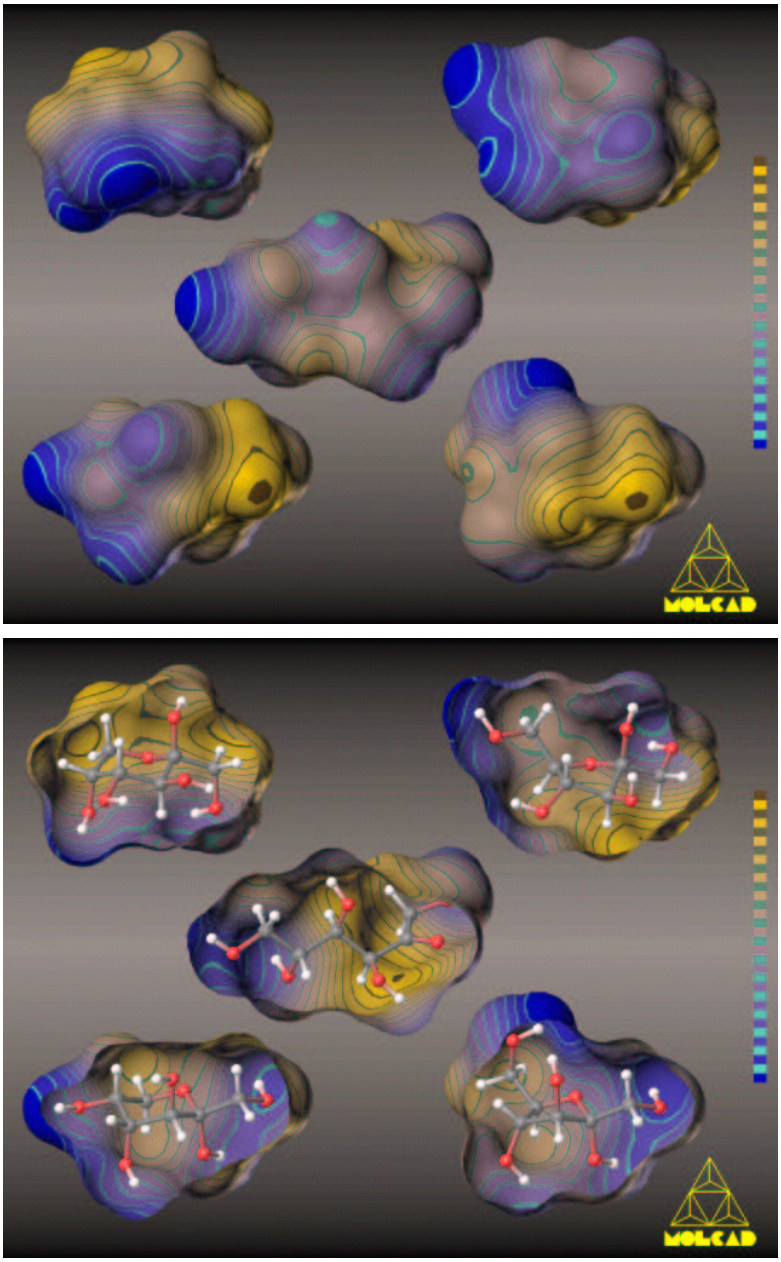


**Fig. 5-16.** Molecular lipophilicity patterns (MLP's) of the fructose tautomers, blue colors representing most hydrophilic, yellow-brown colors most hydrophobic regions (internal scaling for each molecule). The half-opened molecules illustrate the molecular orientation.

Due to ring inversion to the $^{5}C_{2}$-conformation, the three-dimensional arrangement of possible hydrogen bond donor and acceptor functionalities is different in α-D-fructopyranose: the steric properties of diaxial 3,4-diol structure as well as of the axial-equatorial 4,5-OH groups differ substantially from the proposed diequatorial AH-B-couple (3-OH and 4-OH) in β-D-fructopyranose, thus making it improbable that the α-form – this argumentation not only applies to the a-pyranose, but in an analogous fashion also to both the furanoid isomers and the *keto*-form – interacts with the same type of sweetness receptor as the β-pyranose does.

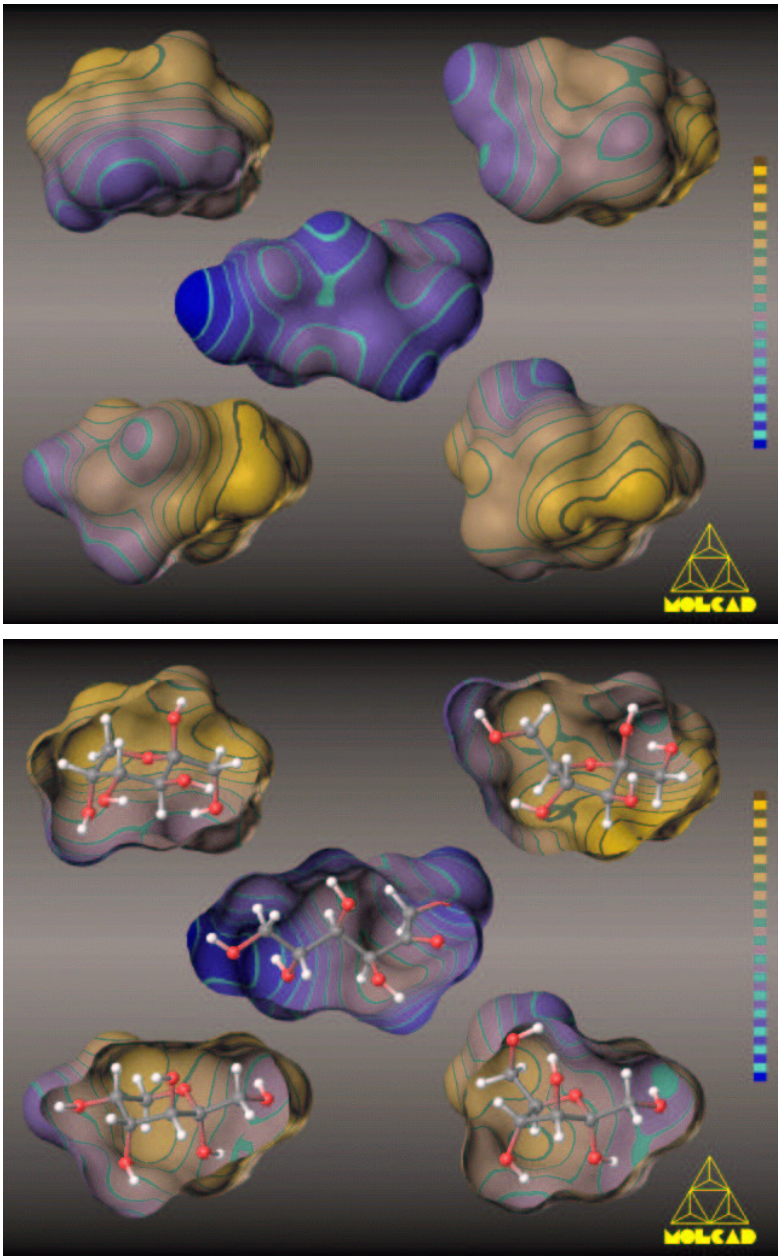

**Fig. 5-17.** Molecular lipophilicity patterns (MLP's) of all fructose tautomers. The color-code applied here is the same for all molecules (MLP ranging from -0.085 to -0.033 in arbitrary units). The molecular orientations correspond to those of Fig. 5-16.

These conclusions up to the relevance of the diequatorial disposition of the AH-B-couple receive further fortification from sweetness considerations in the case of sucrose, which proved the equatorial glucosyl-2- and 3-OH groups to represent a crucial structural element of this compound in the process of sweetness elicitation[19] (Chapter 2 and 3).

Additional corroboration for this hypothesis can be derived from the MLP's presented in Fig. 5-16. In either of the α-*p*-, β-*f*-, and α-*f*-form the most hydrophobic surface areas are directly related to the exocyclic hydroxymethyl units, the endocyclic $CH_2$-group in the former isomer is considerably less hydrophobic as compared to the

β-pyranose. The *keto*-form itself being even significantly more hydrophilic. The pronounced conformational flexibility of the hydrophobic surface regions and their indefiniteness arising therefrom represent an unfavorable entropy contribution to the free energy of interaction with the sweetness receptor, and in consequence, must lead to lowered sweetness potencies of these isomers.

Supportive evidence for this hypothesis can be obtained from the few fructofuranose derivatives which have been reported to be tasteless or even bitter (cf. Chapter 4). The only exception within this series is 1,6-di-methylthio-β-D-fructofuranose (**131**), being 15 – 20 times sweeter than sucrose (on a molar basis)[184]. Obviously, increasing hydrophobicity associated with the 1- and 6-$CH_2$ groups overcomes their unfavorable flexibility, leading to the enhanced sweetness potency of this compound.

**131**
(very sweet)[184]

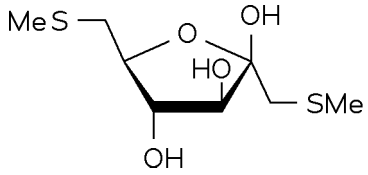


In terms of the early AH-B-assignment to the 1,2-diol grouping of fructose – which should possess almost the same steric arrangement in five- and six-membered rings – the explanation of the lack of sweetness of the furanoid isomers was attempted by the altered stereo geometry of the different rings, the furanose introducing a "barrier between the usual planar relation between AH, B, and X"[93]. Now, on the basis of the MLP's, it becomes improbable that the 1,2-diol grouping represents the AH-B-unit of fructose: in neither of the different tautomers this grouping is located within the most hydrophilic surface region as would be expected for a potential hydrogen bonding system. So far, the location of the AH-B-glucophore in the most hydrophobic molecular parts was observed for none of the common sweeteners[19] (Chapter 2 and 3).

Finally, the low equilibrium proportions of the α-compounds (5 – 10%) and the *keto*-isomer (< 1%) in aqueous solutions rule out any significant contribution of these compounds to sweet tasting properties of fructose.

## Conclusions

In summary, the conformational properties and hydrophobic characteristics of all different fructose tautomers point towards the β-pyranoid form to be the only sweet tasting structure, the others being considerably less important for sweetness

perception, or devoid of any taste at all. Molecular lipophilicity patterns unequivocally identify the surface region ranging from the 6-$CH_2$ to the 1-$CH_2$ grouping (including the ring oxygen atom) to contribute to the hydrophobic interaction with the sweetness receptor.

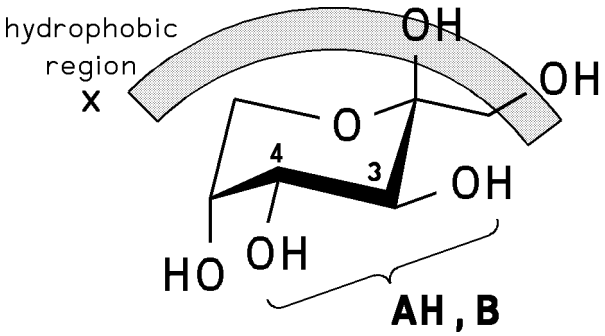


The opposite side located, most hydrophilic molecular surface part is made up by the hydroxyl groups in the positions 3 and 4, which due to their hydrogen bonding capabilities play an important role in sweetness perception.

The results are in accord with the experimental findings of the initially high sweetness after dissolution of the crystalline β-pyranoid form of fructose, and its decrease upon tautomerization into tasteless isomers, i.e. the β-furanose in particular.

Although no ultimate proof of the AH-B-X-assignments could be obtained, the molecular modeling methods applied attest towards the importance of hydrophobic interactions involved in the process of sweetness perception.

## Appendix – Computational Methods

*I. Energy Potential Surfaces and Contour Plots.* All MM- and MD-computations were carried out on the basis of the PIMM88-force field[45] program for in vacuo conditions with a dielectric constant ε equal to 1. Different starting geometries for the calculation of the Φ / Ψ-energy potential surfaces were selected from a permutational analysis of all free exocyclic torsion angles after full energy minimization. The Φ / Ψ-torsion angles of relaxed opposite molecular conformations (pseudoequatorial and pseudoaxial orientations of $C_2$-substituents) were driven in steps of 5 degrees each in the range of ±70° and permutated, extremely high distorted starting geometries ($q > 0.7$, with equal sign of the Φ / Ψ-torsions) were rejected immediately. Both dihedrals were fixed, whilst all other molecular parameters were fully optimized in each step. New ring-geometries were generated from already optimized, conformationally adjacent structures. The self-consistency of the energy matrix was counter-checked by double calculation of structures at same Φ / Ψ-grid points,

generated by different conformational pathways. For each matrix element, the lowest energy conformation emerging from different starting geometries was chosen. Contour plots were computed using cubic regression formulas[163]. The three-dimensional plots of the percentage conformer distribution were derived from the energy matrices according to the Boltzmann-equation at 25°C, neglecting entropy effects. Molecular dynamics simulations (50 ps at 300 K, time step 1 fs, $\varepsilon = 1$) were used to confirm the shape of the energy potential surfaces.

For calculation of the general relationships between $\Phi$ / $\Psi$-ring torsion angles, the Cremer-Pople puckering parameters $\phi$ and $q$[122,123], H-H-torsion angles $\phi$ and $\psi$, and the $^3J_{H\text{-}H}$ coupling constants, different ring conformations were generated by permutational displacement of neighbored atoms of a regular five-membered ring along the *z*-axis perpendicular to the ring plane. During subsequent structure optimization with fixed *z*-coordinates of all atoms to constant bond lengths ($r_{C\text{-}C} = 1.54$ Å, $r_{C\text{-}O} = 1.43$ Å[223]) all angles and torsions were allowed to relax. Hydrogen atoms were placed geometrically assuming idealized tetrahedral geometries for each atom ($r_{H\text{-}H} = 1.00$ Å), and all molecular parameters were calculated and used for the correlations. The NMR-coupling constants were derived from generalized Haasnoot-equations including the effect of $\beta$-substituents[275] for *O*-substituted D-fructofuranoses, with an estimated error of $\sigma_J \approx \pm 0.5$ Hz[275]. The calculated RMS-differences between the couplings of *O*-acyl and OH-free derivatives vary by only $\pm 0.3\,\sigma_J \approx 0.15$ Hz, thus the correlations presented apply equivalently to *O*-substituted and OH-free compounds.

*II. Molecular Surfaces and Hydrophobicity Patterns*. Calculation of the molecular contact surfaces and the respective hydrophobicity patterns was carried out using the MOLCAD[48] molecular modeling program, a detailed description of the computational basics is given in Chapter 3. Color graphics were photographed from the computer screen of a SILICON-GRAPHICS workstation.